Master's thesis

NTNU
Norwegian University of Science and Technology
Faculty of Information Technology and Electrical Engineering
Department of Engineering Cybernetics

Mari Hestetun Dokken
Sandra Garder Løkken

Automated Detection and Removal of EEG Artifacts for an RGB Stimulation-Based Brain-Computer Interface

Master's thesis in Cybernetics and Robotics
Supervisor: Marta Molinas
Co-supervisor: Luis Alfredo Moctezuma
June 2023

NTNU
Norwegian University of
Science and Technology

Mari Hestetun Dokken
Sandra Garder Løkken

Automated Detection and Removal of EEG Artifacts for an RGB Stimulation-Based Brain-Computer Interface

Master's thesis in Cybernetics and Robotics
Supervisor: Marta Molinas
Co-supervisor: Luis Alfredo Moctezuma
June 2023

Norwegian University of Science and Technology
Faculty of Information Technology and Electrical Engineering
Department of Engineering Cybernetics

NTNU
Norwegian University of
Science and Technology

Preface

This master thesis completes a Master of Technology at the Norwegian University of Science and Technology (NTNU) under the Department of Engineering Cybernetics in the spring of 2023. The project was proposed and supervised by Professor Marta Molinas and was completed in collaboration with Sunnaasstiftelsen. The work presented in this thesis is a continuation of the work done in our specialization projects, [1, 2], completed in December 2022 and January 2023 respectively.

Parts of the second chapter are updated and extended versions of the work done in the specialization projects, [1, 2]. The software implementations are done by the authors using *Python* libraries including *MNE*, and *EEGNet* implementation from [3]. The dataset was recorded at the NeuroImaging facilities at Aalto University in Helsinki [4].

The code implemented by us can be shared by contacting us at mari.h.dokken@gmail.com or sandragarder@hotmail.com.

The main contribution of this thesis is the investigation of different denoising techniques for Ocular Artifacts (OA)s suitable for real-time applications. The results can be used in future work toward developing communication systems for people with Locked-in Syndrome (LIS), where Brain-Computer Interface (BCI)s are one of the few possibilities for communicating with the world.

We had little prior knowledge and experience about the human brain or Electroencephalography (EEG) signals as well as little experience with data processing and deep Convolutional Neural Network (CNN) for classification. This thesis hopefully reflects the amount of knowledge we have gained over the past year.

Trondheim, June 2023
Mari Hestetun Dokken & Sandra Garder Løkken

Acknowledgements

Throughout the research, implementation, and writing of this thesis, we have been fortunate to receive invaluable support and assistance. We extend our deepest appreciation to our supervisor, Professor Marta Molinas, for proposing this project and introducing us to the truly fascinating field of BCI and their applications. Her guidance and passion for the project have been instrumental and sincerely inspiring.

We would also like to thank Dr. Luis Alfredo Moctezuma for his patience and guidance, for making himself available for insightful discussions, and for providing valuable feedback throughout the development of this thesis. His expertise and support have been significant in shaping our understanding and enhancing the quality of our work.

Sandra would like to thank her parents and her sister for their unconditional support throughout her studies. She is also appreciative of her friends, especially her fellow students, who have both shared memorable moments during their studies and provided continuous motivation throughout her academic journey. Lastly, she would like to acknowledge her co-author for her insightful contributions, collaborative spirit, and dedication to our shared research.

Mari would like to thank her friends and family for their unwavering love and support throughout her academic journey, and for always being available to listen and inspire. Finishing her studies would not have been possible without her fellow students, providing laughter and encouragement these past five years. Last, but not least, she wished to thank her co-author for being an excellent partner and motivator throughout the completion of this project.

Additionally, we want to express our gratitude to the Department of Engineering Cybernetics for the resources and opportunities provided throughout our academic journey. Finally, we would like to extend our thanks to our fellow students for their motivation, and shared moments of laughter, which have made the past five years engaging and memorable.

Abstract

This thesis investigates methods for removing Ocular Artifacts (OA)s from recorded Electroencephalography (EEG) signals and evaluates their effectiveness and feasibility for use in a Brain-Computer Interface (BCI) system. The motivation stems from the desire to improve the quality of life for persons with Locked-in Syndrome (LIS), a condition where individuals remain conscious and awake but experience complete paralysis, preventing them from moving or communicating. Artifact handling is vital for BCIs to ensure accurate interpretation of brain signals and reliable performance.

A communication system has been proposed in earlier contributions to the project, where a control signal is to be obtained by recording EEG signals generated during a specific visual stimulation protocol [5]. To introduce OA handling into this pipeline, four different techniques were tested: Independent Component Analysis (ICA), an algebraic approach, and two versions of Signal-Space Projection (SSP). These methods were compared in terms of their artifact removal performance and subsequent classification using a Convolutional Neural Network (CNN). The dataset used has EEG data from 31 subjects observing RGB colors on a screen with gray pauses in between. This allowed for binary classification of rest (gray screen) and task (RGB colors).

The experiments performed in this project aimed to evaluate the effects of the different artifact removal techniques and their impact on classification performance. Based on visual inspection of the signal and coherence analysis between the processed signals and the original recordings, it was found that most of the methods effectively detected and removed the OA spikes to a satisfactory degree. However, the algebraic method performed poorly, with variations in OA detection across different channels resulting in either too few artifacts removed or unnecessary removal in non-artifact areas. This discrepancy was also reflected in the classification results, as the other models achieved average accuracies ranging from 69% to 75%, while the algebraic method behaved close to a random classifier at 50%. Out of the real-time appropriate removal methods, the modified SSP method provided the highest average accuracy of 71%. However, variation in the classification made the best individual subject performance 94%, using no OA removal.

The results emphasize the significance of exploring various classifiers and their response to OA removal. It is clear that although further enhancements are needed, the findings demonstrate the viability of developing efficient methods for removing OAs in BCIs, which could improve the classification and prediction performances, thereby facilitating accurate communication platforms.

Abstract - Norwegian

Denne oppgaven undersøker metoder for å fjerne okulære artefakter (OA) fra registrerte EEG-signaler og evaluerer deres effektivitet og gjennomførbarhet for bruk i et fremtidig hjerne-datamaskin grensesnitt (BCI). Motivasjonen stammer fra ønsket om å forbedre livskvaliteten for personer med locked-in syndrom (LIS), en tilstand der personer er bevisste og våkne, men opplever total lammelse som hindrer dem fra å bevege seg eller kommunisere. Håndtering av artefakter er avgjørende for å sikre nøyaktig tolkning av hjerneaktivitet og pålitelig systemytelse for BCIer.

Et kommunikasjonssystem ble foreslått i et tidligere prosjekt, der EEG-signaler generert under en visuell stimuleringsprotokoll blir brukt. For å introdusere OA-håndtering i prosessen, ble fire ulike teknikker testet: uavhengig komponentanalyse (ICA), en algebraisk tilnærming, samt to versjoner av signalromsprosjeksjon (SSP). Disse metodene ble sammenlignet med tanke på deres evne til å fjerne artefakter og påfølgende klassifisering ved hjelp av et konvolusjonelt nevralt nettverk (CNN). Datasettet som ble brukt i denne oppgaven inneholder EEG-data fra 31 deltakere, spilt inn mens de observerte en skjerm som viste RGB-farger i intervaller med en grå pause mellom hver farge. Denne oppsettet muliggjør en binærklassifisering av hvile (grå skjerm) versus oppgave (RGB-farger).

Eksperimentene som ble utført i dette prosjektet hadde som mål å evaluere effekten av de ulike artefaktfjerningsteknikkene og deres innvirkning på klassifisering. Basert på visuell inspeksjon og kohæransanalyse av de bearbeidede signalene og de opprinnelige opptakene, ble det funnet at de fleste metodene effektivt oppdaget og fjernet OA-spike på en tilfredsstillende måte. Imidlertid fungerte den algebraiske metoden dårlig med variasjoner i OA-deteksjon mellom ulike kanaler, noe som resulterte i enten for få fjernede artefakter eller unødvendig fjerning i ikke-artefaktsområder. Denne forskjellen ble også gjenspeilet i klassifiseringsresultatene, da de andre modellene oppnådde gjennomsnittlig nøyaktighet på 69% til 75%, mens den algebraiske metoden oppførte seg som en tilfeldig klassifiserer med 50% nøyaktighet. Av fjerningsmetodene som er egnet for sanntidsbruk, ga den modifiserte SSP-metoden den høyeste gjennomsnittlige nøyaktigheten på 71%. Imidlertid resulterte variasjonen i prestasjon i den beste individuelle klassifiseringen på 94%, uten bruk av OA-fjerning.

De oppnådde resultatene understreker betydningen av å utforske ulike klassifiseringsmetoder og deres respons til metoder for fjerning av OAer. Det er tydelig at selv om ytterligere forbedringer og optimalisering er nødvendige, viser funnene at det er mulig å utvikle effektive metoder for å fjerne okulære artefakter i BCIer, og dermed bistå i utviklingen av nøyaktige kommunikasjonsplattformer.

Contents

List of Figures

List of Tables

Acronyms

BCI Brain-Computer Interface

CLIS Complete Locked-in Syndrome

CNN Convolutional Neural Network

DWT Discrete Wavelet Transform

ECG Electrocardiogram

EEG Electroencephalography

EOG Electrooculogram

FgMDM Minimum Distance to Mean with geodesic filtering

FIR Finite Impulse Response

FN False Negative

FP False Positive

ICA Independent Component Analysis

LIS Locked-in Syndrome

LOOM Leave-one-out Model

MAD Median Absolute Deviation

MEG Magnetoencephalography

ML Machine Learning

NN Neural Network

OA Ocular Artifacts

PNS Peripheral Nervous System

RF Random Forest

SD Standard Deviation

SSP Signal-Space Projection

SVM Support Vector Machine

UT Universal Threshold

V1 Primary Visual Cortex

V4 Visual Area 4

Chapter 1

Introduction

LIS is a neurological disorder that results in quadriplegia and anarthria, meaning a partial or complete loss of voluntary muscle control and speech, respectively. Individuals affected by LIS remain conscious and have intact cognitive functions, but they cannot communicate verbally or move their bodies, resulting in a state of being "locked in" [6]. There are varying degrees of LIS, with some individuals having partial voluntary muscle control over certain body parts, such as lip twitches or neck movements, while others experience complete paralysis, including eye movement. However, even in the most severe cases, cognitive function and sensory abilities such as hearing, smell, taste, and the ability to experience pain and pleasure remain intact [7].

In addition to the physical challenges faced by individuals with LIS, their inability to communicate highly affects their quality of life. Due to the anarthria, their communication possibilities are reduced to the movement they are able to produce. Although several communication methods are available today, they are often limited in various ways. For instance, eye-tracking with a spelling board is one of the methods used today [8]. It will enable the person to express themselves, however, it comes with a large delay from when the thought appears to when the spelling is finished and the message is conveyed. "I hate that delay. I want to answer right away because the sentence is clear in my head." [9] is how a 21-year-old LIS patient using eye-tracking describes the communication process, highlighting the frustration and limitations he experiences when using this method. Keeping up conversations in this manner is tedious and inefficient, making conversations time-consuming and exhausting, which can lead to social exclusion. Moreover, gaze-dependent communication requires the ability to control eye movements, and losing that control means losing the ability to communicate. For those with Complete Locked-in Syndrome (CLIS), this method is not possible due to complete paralysis[8].

Moreover, individuals with the mentioned condition frequently encounter stigmatization and discriminatory treatment as a result of insufficient understanding regarding their condition [8]. Instead of engaging with the person affected, people may talk around or over them or exclusively direct their communication to the caregiver. This communication exclusion not only causes frustration for those

with LIS but also perpetuates misconceptions about the disease, deepening the societal misunderstanding and isolation of those affected, affecting their everyday life.

Therefore, it is crucial to develop and improve communication methods to enhance the quality of life and well-being of individuals with LIS. BCI systems use brain activity as input to a computer application. The EEG signals from the brain can be used by Machine Learning (ML) algorithms calibrated to the user, allowing the user to control a computer with their mind. This can possibly make a more efficient way of communication. Since the cognitive function is one of the few functionalities that remains unaffected by the disease, this enables a communication system suitable for all stages of the disease. BCIs also have the potential to improve communication efficiency for individuals with LIS, which can possibly lead to reducing the social exclusion people with LIS experience today by making it easier to engage in conversations [8, 10].

1.1 Motivation

The purpose of this work is to explore the possibility of creating a communication system for individuals with LIS based on EEG and to investigate feasible methods to achieve this. Previous contributions to the project [5, 11], have explored the possibility of using a combination of the brain's color perception and the eye movement of the user to control a BCI. During these experiments, participants were exposed to different colors while their EEG data was collected. This data was used to train ML models capable of predicting the specific color exposure when presented with new, unseen data. Several processing pipelines were explored, including varying data processing, feature extraction, and classification models. Notably, an average accuracy of 74.3% and 61.4% was achieved in differentiating between a task and resting state, and between the four colors expositions, respectively.

The author suggested that the presence of OAs could have been a contributing factor to the end result. Removal of OAs is usually done offline, as the state-of-the-art methods for removal are computationally heavy and therefore not real-time suitable [12]. However, the presence of OAs in EEG data could significantly reduce the reliability of BCI systems. Therefore, in the work towards a communication platform for people with LIS, investigation of the effectiveness of OA removal methods suitable for real-time applications, such as BCIs, is of importance.

1.2 Problem Description

This work aims at automatically removing OAs from EEG signals by using three different techniques. The performance of the methods will be evaluated on the possibility of being used in a future BCI. The second objective is to train different Neural Networks, using the processed datasets, and compare their performance.

1.3 Approach

The approach involves using four different techniques to remove eye blink artifacts from EEG data; ICA, two versions of SSP, and an algebraic method. These techniques will be compared in terms of

their ability to remove eye blink artifacts and improve the classification performance of a CNN. The performance of the four processed datasets will be compared to evaluate the effectiveness of each technique.

1.4 Outline

The introduction of the general problem and the objectives of the work is done in chapter 1. Chapter 2 provides relevant background information, on signals from the brain and different data processing techniques. A brief overview of previous research on BCIs for LIS and the methods for signal processing is given in chapter 3, while chapter 4 presents a description of the specific implementations and pipelines utilized in this work. In chapter 5, the experiments conducted, and their corresponding results, are presented. Finally, chapter 6 offers a discussion of the obtained results and provides recommendations for future work.

Chapter 2

Background

2.1 Locked-in Syndrome

LIS is a neurological disorder caused as a result of injury to the brain stem. There are multiple potential causes of injury, including but not limited to stroke, hemorrhage, trauma, and hypotension [13]. This part of the brain contains motor nerves responsible for controlling the voluntary movement of the body and facial muscles. As a result, LIS is mainly characterized by quadriplegia and anarthria, with the patient often retaining vertical movement of the eyes as well as control of the upper eyelid. Patients also maintain their cognitive abilities intact, resulting in individuals that are present and awake without the opportunity to express themselves through easy communication [14, 15].

LIS is typically divided into three classifications: 1) Classical LIS is characterized by the individual being completely immobile except for vertical eye movements and blinking. 2) Partial LIS allows for some voluntary motor functions, while 3) CLIS is the most severe form and results in total paralysis, rendering a person completely immobile and unable to communicate [16]. It's worth noting that a person with LIS may eventually progress to CLIS.

2.2 The Anatomy of the Human Brain

The human brain regulates all bodily functions, including cognitive and behavioral processes. It is typically divided into three primary regions based on the functions controlled in those regions: the cerebrum, the brainstem, and the cerebellum. The brainstem is located at the base of the brain and connects the brain to the spinal cord. The brain and the spinal cord make up the central nervous system. Together, they are responsible for integrating all sensory information from the Peripheral Nervous System (PNS). The brain processes the information about the current state of the body, and together with past experiences, it directs motor responses through the PNS. Above the brainstem, the cerebellum is located, which coordinates movement and maintains balance while also contributing to cognitive functions such as attention and language. The largest part of the brain, the cerebrum, consists of two hemispheres which are further divided into four lobes, shown in fig. 2.1. The occipital

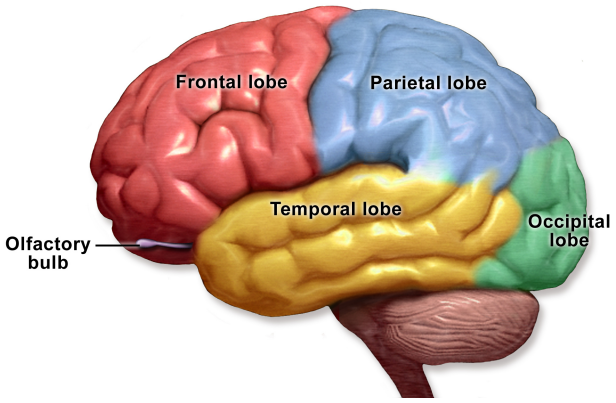

Figure 2.1: Illustration of the four lobes in the cerebrum. Reprinted from [18].

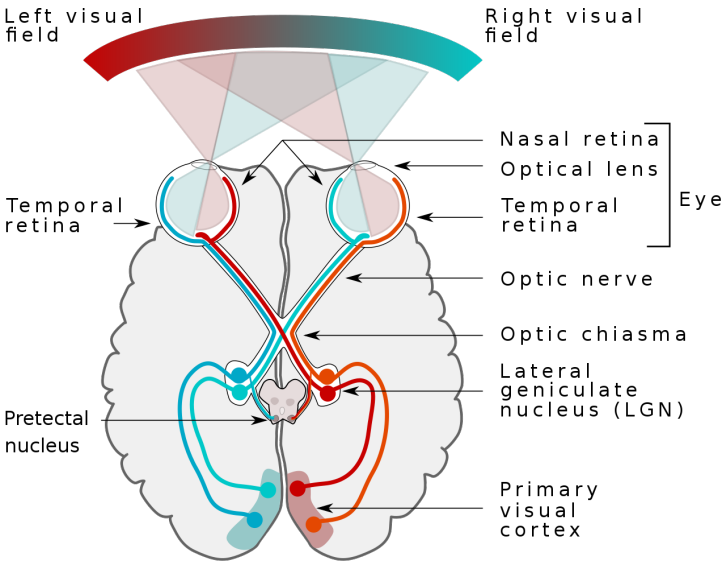

Figure 2.2: Illustration of the visual pathways through the brain. Reprinted from [23]

lobe is mainly the part of the cerebrum that processes visual signals [17].

2.2.1 Color Perception in the Brain

When light from the environment and light sources enters the eye, it is captured by the cone and rod photoreceptors in the retina at the back of the eyeball. These photoreceptors convert the light energy into electrical signals, which are then carried by neurons through the optic nerve to the Primary Visual Cortex (V1) in the occipital lobe for signal processing, visualized in fig. 2.2 [19]. There are three types of cones, each sensitive to different ranges of wavelengths of light: short (S), medium (M), and long (L) wavelengths, corresponding to blue, green, and red light, respectively [20]. By comparing the signals from the different types of cones, the brain is able to determine the perceived color of an object [21]. Depending on the information being processed, the visual pathway may differ. Visual Area 4 (V4) in the occipital lobe, the purple area in fig. 2.3, is believed to be the primary processing center for color perception [22]. That means that this is the area mostly stimulated when observing color.

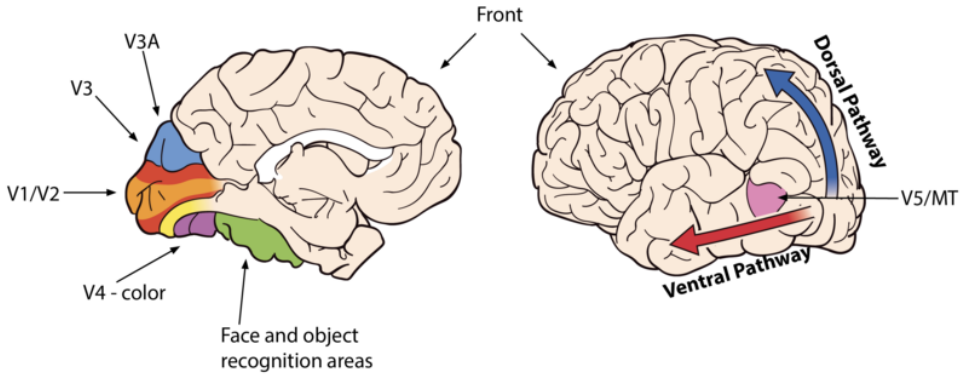

Figure 2.3: Illustration of the visual areas in the brain. Reprinted from [24]

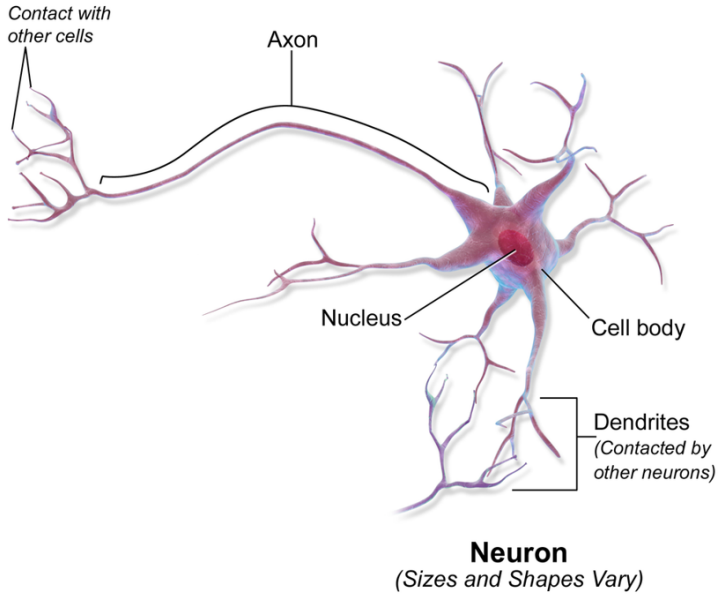

Figure 2.4: Anatomy of a neuron. Reprinted with modifications from [18].

2.3 Signals of the Brain

In the brain, communication is achieved through electrical and chemical signals in a process called neural communication. The anatomy of a neuron is illustrated in fig. 2.4. An electrical signal, called an action potential, travels down the axon of a stimulated neuron to the axon terminal where it triggers the release of chemical neurotransmitters [25]. These neurotransmitters cross the synapse and bind to receptors on the dendrites of the next neuron, causing ion channels to open or close and creating a new electrical signal. This signal transmission repeats, ultimately transmitting information throughout the brain. The resulting electrical stimuli can be measured and analyzed to gain insight into the functioning of the brain [19].

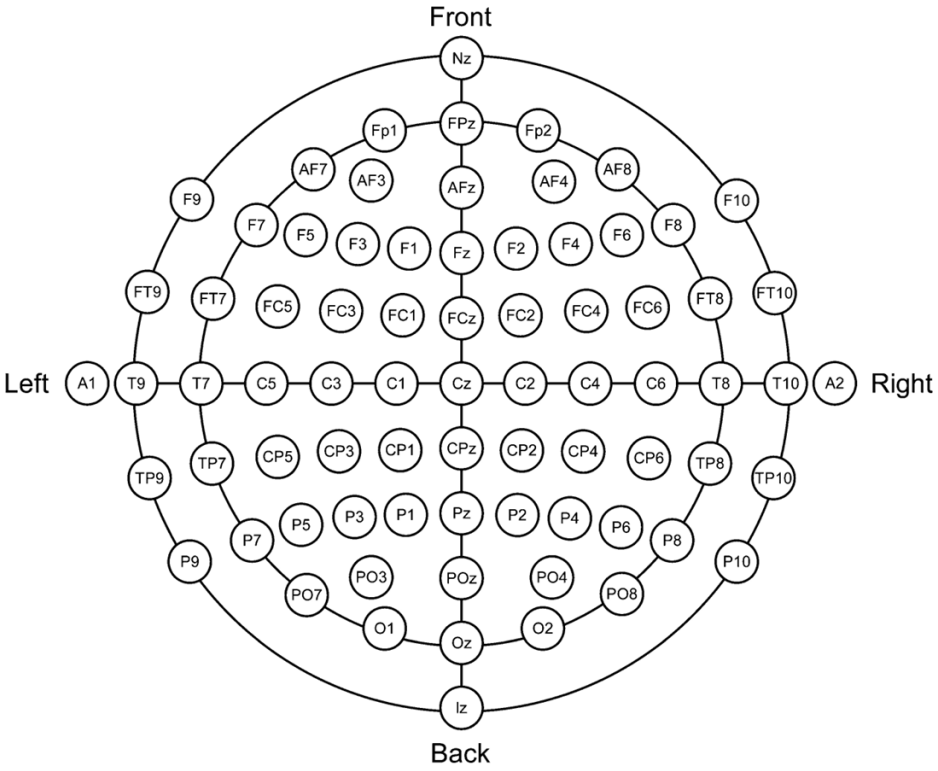

Figure 2.5: The international 10-20 system for electrode placement. Reprinted from [26]

2.3.1 Electroencephalography

EEG is a non-invasive technique employed to measure the electrical activity of the brain. The process involves placing electrodes on the scalp to detect the electrical signals produced by neurons. For the signal to be detected by the electrode, it has to pass through the meninges, the skull cerebrospinal fluid, and the skin. All of these barriers have a distinct level of resistance, meaning that the signals recorded have to be a sufficient amount of accumulated post-synaptic firings happening concurrently and in the same direction. Greater synchronization of postsynaptic potentials results in larger EEG amplitudes and lower frequencies [27]. The resulting EEG dynamics are highly nonlinear and complex [28]. In order to reduce the resistance between the electrode and the scalp, and thereby improve the quality of the measurements, a conductive gel can be used.

2.3.2 Signal Acquisition

The presence of electrical interference from the body, such as muscle contractions, or external sources like power lines, can make it challenging to analyze non-invasive EEG data, as these signals can mask or attenuate the recorded signal. To address this issue, differential amplifiers are used to eliminate biological and ambient noise in EEG recordings [29]. There are different options for choosing the reference electrode. In monopolar EEG recordings, a distant reference electrode is compared with the measuring electrode to ensure that only the signal of interest is extracted and amplified while the common noise is rejected [30]. However, this method can be affected by variations in the electrical properties of the scalp and the tissues underlying the electrodes, as well as by the distance between the reference electrode and the scalp. These factors can lead to inconsistencies and errors in the EEG

recordings. To overcome these limitations, a virtual reference node can be implemented instead of a distant reference node. This is done by averaging the signals from all electrodes, excluding the one being used as the measuring electrode. This method allows for capturing more localized changes in the electrical activity of the brain [31].

Each electrode in EEG recordings captures a signal from a particular region of the brain. The scalp electrodes can be positioned in various ways, and there can be difficulties with placing them correspondingly on different subjects due to anatomical variations. The International 10-20 System for electrode placement provides a standardized system for electrode placement, based on four defined anatomical landmarks in the front, back, left, and right of the head. Each electrode is placed with an interval of 10 or 20% of the total latitudinal and longitudinal lines [26]. Each electrode is assigned a name consisting of a letter and a number, where the letter indicates the corresponding brain region (such as 'Fp' for frontal pole, 'F' for frontal, 'C' for central, 'P' for parietal, 'O' for occipital, and 'T' for temporal), and the number indicates the distance from the middle line, where odd and even numbers represent the left and right lobe, respectively. This convention is illustrated in fig. 2.5.

2.3.3 Frequency Bands

The synchronized and asynchronized firing of neurons causes EEG to have a large range of frequencies. Waveform frequencies contain information about in which state the subject is, such as wakefulness or sleep [32]. The frequencies are normally divided into five categories, named with the Greek letters $\delta, \theta, \alpha, \beta$, and γ. There is no consensus in the literature on the defined frequency ranges. The values presented in table 2.1 are the ones most commonly used by clinical electroencephalographers [33]. Each of the bands is associated with different cognitive states of the brain. In the occipital lobe electrodes, alpha rhythms are expected to achieve their highest values [33]. Generally, frequencies in the γ band are rarely encountered in the scalp EEG [32].

There are several issues associated with the division of frequency bands in EEG signals. Firstly, there is a lack of agreement on the specific frequency ranges for each band, which can vary among studies and hinder cross-study comparisons. Secondly, the division of frequency bands may oversimplify the complex nature of EEG signals, which consist of multiple overlapping and interdependent frequency components. Consequently, such division may obscure the underlying dynamics and interactions between different frequency components. Thirdly, the interpretation of frequency bands can be subjective and context-dependent. The same frequency band may have different meanings depending on the cognitive or behavioral state of the subject, and the task being performed, in addition to other factors [32].

2.3.4 EEG Artifacts

The EEG signal can be affected by extraneous or unwanted signals, known as artifacts, which can complicate the accurate interpretation of brain activity. These artifacts fall into two categories: physiological and non-physiological. Physiological artifacts are generated by electrical disturbances in the body, such as cardiac activity, respiration, perspiration, eye movement, and blinking. Non-physiological artifacts arise from external sources, such as electrode or cable movement, body movements, or

Frequency band	Frequency band	Associated with
Delta (δ)	0.1 – 4 Hz	Homeostatic sleep drive
Theta (θ)	4 – 8 Hz	Homeostatic sleep drive, relaxed, meditative, and creative states
Alpha (α)	8 – 13 Hz	Relaxed wakefulness and drowsiness
Beta (β)	14 – 30 Hz	Active thinking
Gamma (γ)	> 30 Hz	Cognitive states

Table 2.1: Frequency bands of the brain activity [33] and their association [32].

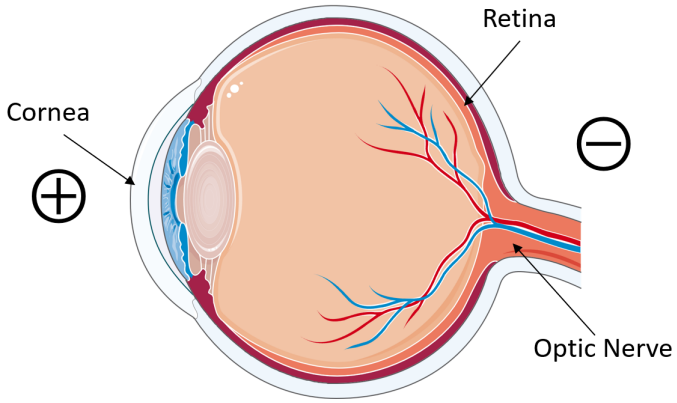

Figure 2.6: The human eyeball with the polarization indicated. Reprinted with modifications from [36].

electrical and electromagnetic interference [34].

Ocular Artifacts

OA in EEG pertain to electrical signals generated by eye movements or blinks, which are predominantly observed in the frontal region and can significantly vary across individuals, resulting in alterations in signal amplitude [35].

There exists a voltage difference between the cornea and the retina as depicted in fig. 2.6, resulting in the eye acting like a dipole, thereby creating an electrical field. As the eye rotates, the field fluctuates, leading to a detectable alteration in voltage that can be captured by electrodes positioned close to the eyes [37]. These artifacts are commonly visible during saccadic eye movement, meaning movement caused by changing the point of fixation. This could be from larger movements resulting in larger amplitudes and lower frequencies, such as moving over a landscape, or from smaller movements, such as reading a book, which would give smaller amplitudes and higher frequencies. An example of how such rapid eye movement presents itself in EEG data is given in fig. 2.7. These saccadic artifacts are particularly evident in the channel data at the top of each chain, meaning the channels that are the closest to the eyes. Here, the small spike-like discharges corresponds well with the recorded Electrooculogram (EOG) data at the bottom.

Artifacts that stem from blinking and vertical eye movement are significantly impacted by the eyelid.

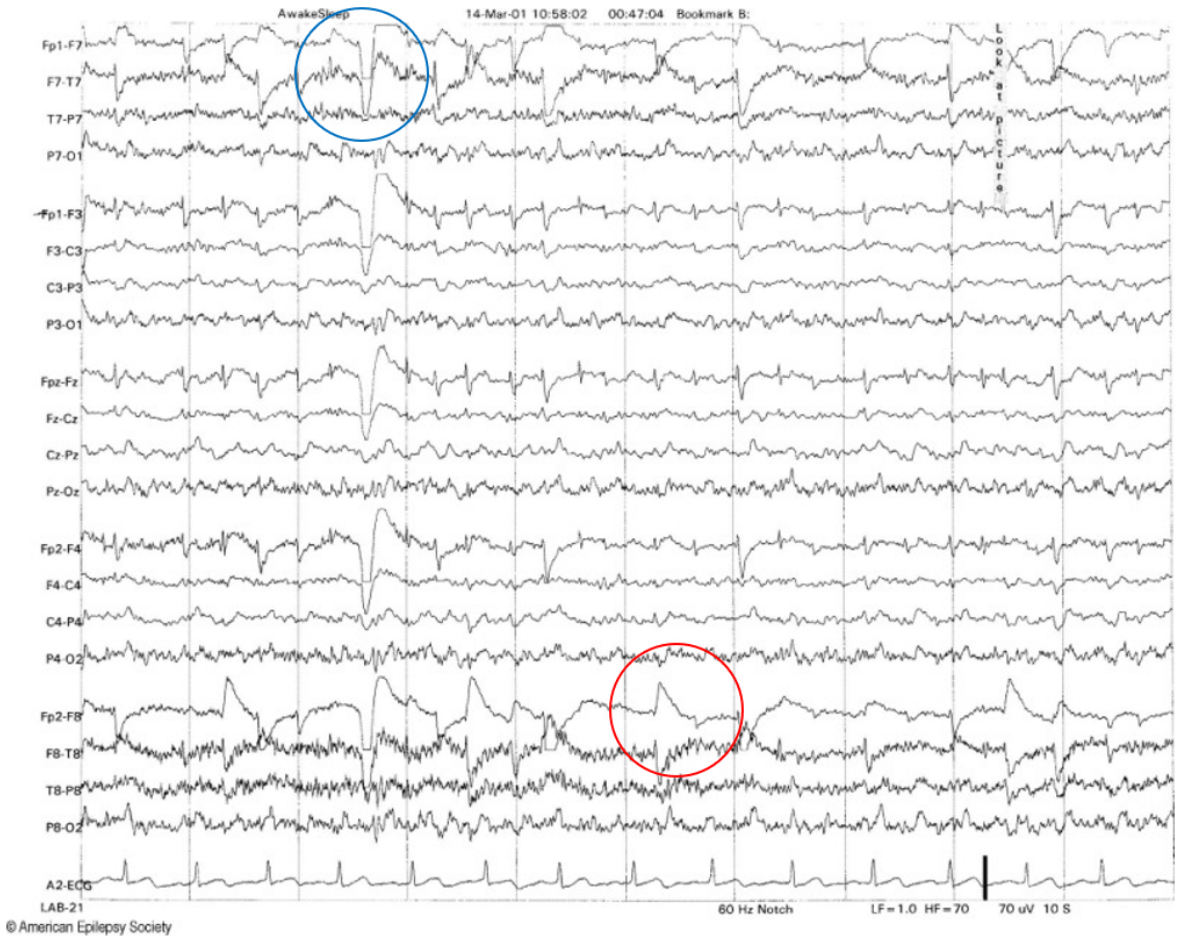

Figure 2.7: An example of how OAs from rapid eye movement presents itself in EEG data. Each vertical division shows 1 second. The first four channels form a chain from over the left temporal head region, and the second four form a chain over the left parasagittal head region. The bottom two chains form over the corresponding right parasagittal and temporal regions, respectively. The middle set of four channels shows the data recorded over the midline head region. The final bottom channel shows EOG data recorded on the right side. Reprinted with modifications from [30]. The blue circle illustrates an OA from a blink, while the red circle is an example of rapid eye movement.

The lid movements can be seen as 'sliding electrodes' that short circuit the positive charge of the cornea to the extra-ocular skin [39]. This means that when the eyelid closes, the overall electrical potential difference between the retinal and corneal sides of the eyeball will be determined by the combined values of the retinal and corneal potentials, thus altering the EEG signal with a substantially larger amplitude than that of the saccades [40]. An example of this can be seen in fig. 2.8 where both slower eye movement and eyelid artifacts are included along with an example of muscle tension. The three examples display significantly different shapes, amplitudes, and frequencies.

The frequency bands associated with OAs have been explored in various studies, revealing some variations in their categorization. According to one source [41], EOG artifacts span a frequency range of 0-12 Hz. Another study [42] focuses specifically on blink artifacts, suggesting their frequency range extends up to 13 Hz. In contrast, a third source [43] proposes a more detailed classification, distinguishing between eyelid artifacts (0-4.5 Hz) and saccadic movement artifacts (4-20 Hz). These differ-

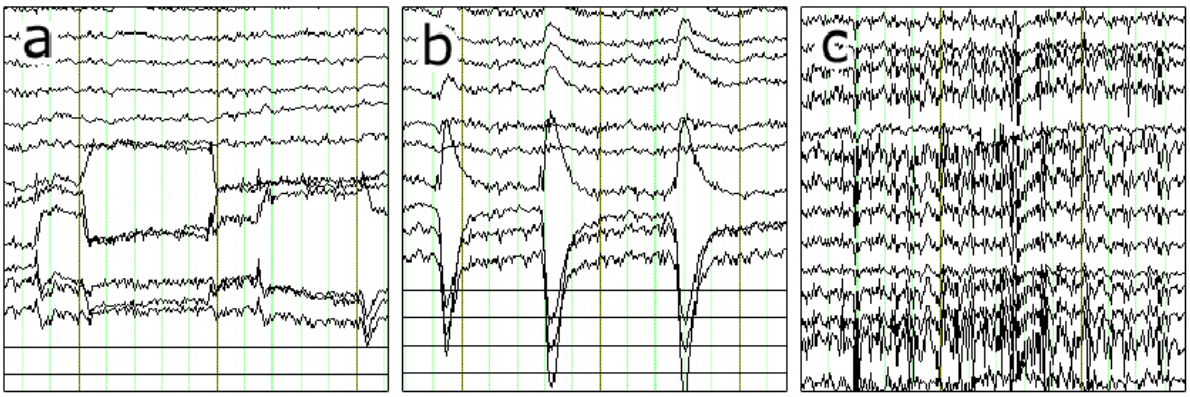

Figure 2.8: Examples of physiological artifacts in EEG recording. a) eye movement, b) eye blink, and c) muscle tension. In contrast, normal EEG signals typically exhibit lower amplitudes, which can be observed in the unaffected channels located in the upper portion. Reprinted from [38]

ences in frequency band characterizations suggest that the manifestation and characteristics of OA can vary across different types of ocular activity. Understanding these distinctions is crucial for effectively identifying and mitigating the impact of OAs in various applications, such as signal processing and data analysis.

2.4 Preprocessing

As mentioned, the raw EEG data is susceptible to noise and disturbances that can hinder the accurate interpretation of brain activity. Preprocessing the EEG data plays a vital role in removing these disturbances, improving the signal-to-noise ratio, and facilitating the detection of subtle changes in brain activity. This is a critical step in ensuring that the data is suitable for further analysis [44].

Bandpass Filter

A bandpass filter refers to an electronic filter that allows a specific range of frequencies, known as the passband, to pass through the filter while rejecting frequencies outside that range, known as the stopband. In other words, a bandpass filter attenuates signals with frequencies lower or higher than the passband, effectively filtering out unwanted frequencies.

Notch Filter

A notch filter refers to a type of signal processing filter that is used to remove or reduce the amplitude of a specific frequency or range of frequencies within a signal. This is achieved by applying a band-stop filter, which attenuates a specific range of frequencies while allowing all other frequencies to pass through unaffected. In the context of this project, it is used to remove the 50 Hz common-mode noise, to enhance the signal-to-noise ratio, and improve the overall data quality.

2.5 Data Processing

The OAs introduce high-amplitude signals to the EEG data that can distort the underlying neural activity patterns. This section focuses on methods specifically designed for removing such spikes. The algebraic method used in this work encompasses multiple steps, including the application of a Finite Impulse Response (FIR) filter, spike detection, and Discrete Wavelet Transform (DWT). Two approaches utilize SSP, while the final method involves the use of ICA.

2.5.1 Finite Impulse Response Filter

FIR filters are digital filters that generate an output of limited length when presented with a finite-length input, like an impulse. The filter's frequency response is defined by a collection of coefficients [45].

$$y[n] = \sum_{k=0}^{N-1} h[k]x[n-k] \tag{2.1}$$

Equation (2.1) shows the filter's formula, where the output signal of the filter is obtained by taking the weighted sum of the input signal $x[n]$, with the weights determined by the impulse response of the filter, $h[k]$. When the FIR filter is linear, its coefficients exhibit either symmetry or anti-symmetry. Consequently, the number of multiplications required is reduced by half the length of the filter, which is equal to $(N+1)/2$ for filters with odd values of N [46].

2.5.2 Spike Detection

The following spike detection algorithm is presented in [47]. Consider a time interval $I = [\tau, \tau + T]$ of period T at timestamp τ. In this interval, it is assumed that there is at most one blink. A FIR filter of order M is applied to the noisy signal $y(t)$ in this interval, using the sliding window technique, with window size L, repeated n times in the interval I. The result is on the form

$$a_k t_k^2 + b_k t_k + c_k = 0 \tag{2.2}$$

where the coefficients are the output of the filter at time t_k. If all three coefficients are non-zero, there is a discontinuity in the signal at that timestamp. This corresponds to a spike in the signal.

To decide if there is a spike at timestamp t_k, a decision function can be compared to a threshold value. The decision function for the signal $v_k(\tau)$, based on the n sliding windows in the interval with length T, can be expressed as

$$F_n = \prod_{k=0}^{K-1} F_{k,n} \quad \text{for} n = 0, 1, 2 \ldots \tag{2.3}$$

where

$$F_{k,n} = \left[v_{k+1,n}\right]^2 - v_{k,n} v_{k+2,n}. \tag{2.4}$$

This can be compared to a threshold to separate normal signal data from spikes. In theory, F_n should

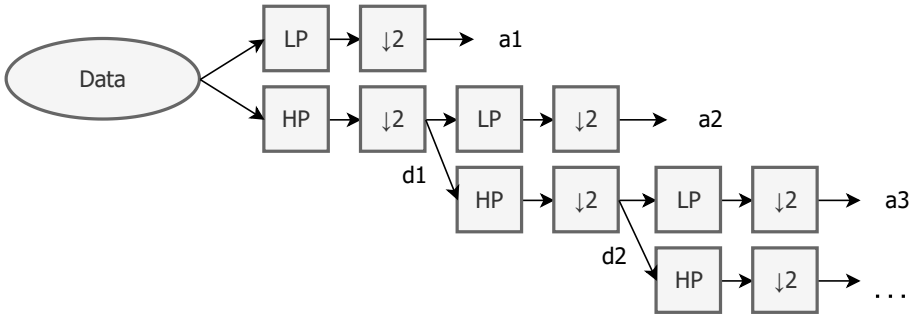

Figure 2.9: Graphical explanation of DWT decomposition. (LP: Low pass filter, HP: High pass filter, ↓2: down sampled by 2, ai: approximate coefficients at level i, di: detail coefficients at level i)

be zero, but to take into account noise it is compared to a fixed threshold.

2.5.3 Discrete Wavelet Transform

DWT is a method in signal processing, where a signal is represented as a linear combination of a set of basis functions, or wavelets. It has been evaluated as a method for real-time processing because of its computational efficiency [47]. By comparing the input signal to the mother wavelet at different translations and scales, the DWT produces coefficients that encode the signal's representation in the wavelet basis. These coefficients encapsulate the signal's time and scale variations, facilitating further analysis and manipulation [48].

The DWT generates coefficients for each decomposition step, with detail coefficients corresponding to high frequencies, and approximate coefficients to low frequencies. Both types are down-sampled by a factor of 2 for each step, as shown in fig. 2.9. The maximum level of decomposition therefore depends on the number of data points and the type of mother wavelet, since down-sampling reduces the coefficients at each level.

$$\gamma_{jk} = \int_{-\infty}^{\infty} x(t) \frac{1}{\sqrt{2^j}} \psi\left(\frac{t - k2^j}{2^j}\right) dt \tag{2.5}$$

Equation (2.5) depicts the general form of the DWT. The mother wavelet is represented by ψ while $x(t)$ is the signal and the parameters j and k correspond to scaling and shifting, respectively. Adjusting the scaling factor of the wavelet alters the sensitivity to changes, enabling customization for either low or high frequencies. Shifting the signal introduces a delay, which changes the time domain of the signal. Some of the most common mother wavelets are shown in fig. 2.10. Selecting an appropriate mother wavelet is crucial and is typically done by choosing a wavelet that resembles the input signal [49].

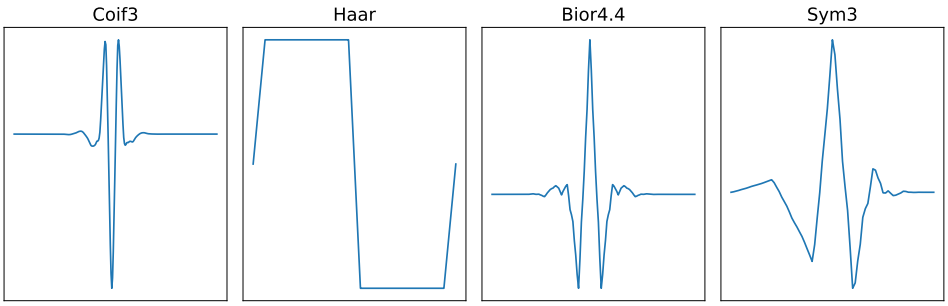

Figure 2.10: Common wavelet basis functions made using the *pywt* library. They are classified by wavelet family and order, e.g. Sym3 = symlet wavelet of the 3^{rd} order

2.5.4 Signal-Space Projection

SSP is a technique commonly employed in EEG for removing noise from recorded signals. The approach involves projecting the signal onto a lower-dimensional subspace, the selection of which entails the calculation of the average pattern across sensors in the presence of noise. This pattern serves as a direction in sensor space, and the subspace is constructed to be orthogonal to this noise direction [50].

When implementing SSP, it is crucial to select the right noise subspace for the projection [51]. If the selected subspace doesn't fully capture the noise pattern, some noise may remain after the projection. Conversely, if the selected subspace is too large, it may also include some of the signals, leading to a reduction in data quality and potential loss of important information. It has also been found that the application of SSP may reduce the output signal itself [51].

The subspace is found by modeling the recorded signal as a combination of the signal $s(t)$ and the noise $n(t)$ as seen in eq. (2.6a). The noise is further expressed in eq. (2.6b) as a column $c(t)$ made up of a subset of field patterns of the noise, its orthogonal basis U, and a small error $e(t)$ which is considered dismissible. The field disturbances $c(t)$ is the term that captures the noise, and it is removed by multiplying by the transform of U. In total, this culminates in P, the output projection expressed in eq. (2.6d) [50].

$$r(t) = s(t) + n(t) \tag{2.6a}$$

$$n(t) = Uc(t) + e(t) \tag{2.6b}$$

$$s(t) = r(t) - n(t) = Pr(t) \tag{2.6c}$$

$$P = I + UU^T \tag{2.6d}$$

This process can be computationally heavy, depending on the size of the data and the computing resources. However, the output is a vector that is to be multiplied with the input signal. This means that applying the projection is a much simpler process.

SSP is primarily used for eliminating stationary environmental noise, caused by external sources beyond the subject's body and the recording system. Nevertheless, the method is also applicable for eliminating biological artifacts resulting from Electrocardiogram (ECG) and EOG activities [52].

2.5.5 Independent Component Analysis

ICA is a mathematical technique used to separate a multivariate signal into statistically independent components. Generally, ICA is a computationally heavy method that requires several rounds of visual inspection and decomposition. It is based on the assumption that the observed signal is a linear mixture of underlying independent sources, where each source signal is non-Gaussian and has a unique probability distribution [53].

ICA works by decomposing the mixed signals into their independent components, which can be identified based on their statistical properties. By assuming there are N statistically independent signals $s_i(t)$, $i = 1, ..., N$ where each signal is a realization of some fixed probability distribution, the observation of the signals $x(t)$ can be formulated as

$$x(t) = As(t) \tag{2.7}$$

where A is the mixing matrix. A formula for the estimated original signals can be found by inverting the formula such that

$$\hat{s}(t) = Wx(t) \tag{2.8}$$

where $W = A^{-1}$. When using ICA as an artifact removal technique, the independent component or components that represent the artifact source is visually identified and used to remove the noise from the signal mixture [53].

When employing the ICA method, there exists a potential risk where the application of correction on channels with comparatively low signal-to-noise ratio, such as EEG channels and channels located farther from the signal peaks, may introduce additional noise to these channels. This occurs due to the elevated errors in estimating the mixing matrix for ICA when the signal-to-noise ratio diminishes [54].

2.6 Classification and Machine Learning

Multi-class classification is a critical task in BCI applications, where EEG signals are classified into several categories. In a BCI system, EEG signals are employed to decode the user's intention or mental state, which is then translated into control commands for an external device. For this project, the classification is done using an ML algorithm, which are algorithms that have the ability to enhance their performance by leveraging previous experiences [55]. This experience can include prior data points that are used to find latent structures and properties within the data. When the data points lack labels or target values, this process is referred to as unsupervised learning. Conversely, when these data points are accompanied by labels or target values, it falls under the domain of supervised

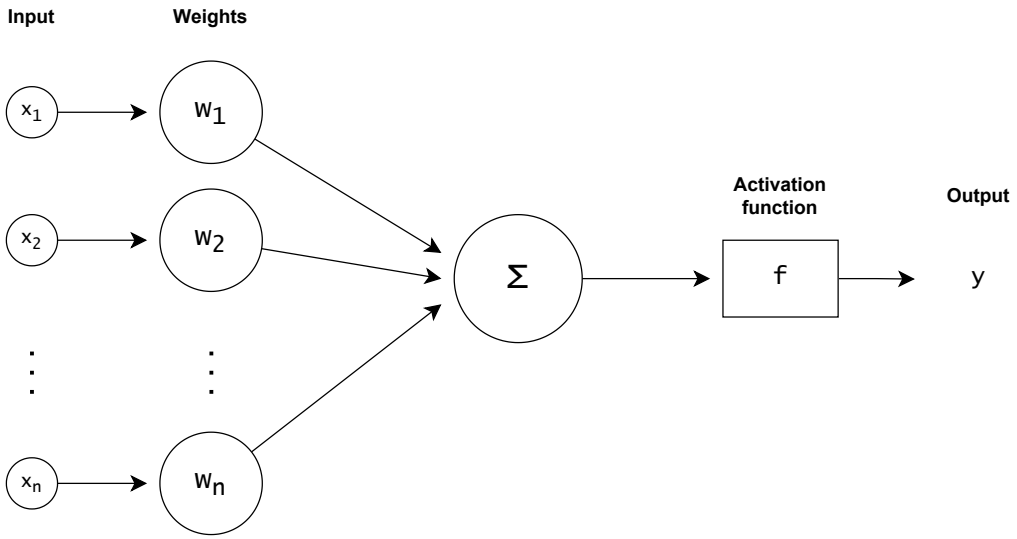

Figure 2.11: Illustration of a single neuron for ML

learning. In the context of this research project, supervised learning techniques will be employed to facilitate the analysis and prediction of the data.

A ML algorithm offers various means to control its behavior in generating prediction models. To determine the optimal values for these controls, the dataset is divided into three subsets: the training set, the validation set, and the test set, which are utilized at different stages of the classification process.

For each ML model constructed, there exist a set of weights, known as parameters, which determine the significance of each feature in the prediction. These parameters are optimized using the training set, resulting in the creation of the best model for the given configuration. The process of generating these models is governed by the algorithm's hyperparameters and is fine-tuned using the validation set [56].

2.6.1 Neural Networks

Neural Network (NN) are a type of ML algorithm that consists of interconnected processing units, or neurons, that work together to learn from data [55]. These neurons receive input from other neurons, process the input by attaching weights, and produce an output that is transmitted to other neurons. The process of a single neuron is shown in fig. 2.11. NN have demonstrated their effectiveness in various tasks, including classification [57]. The learning process of NN involves backpropagation. This means that the error between the predicted output and the actual output is propagated back through the network and used to adjust the weights of the neurons [58]. As a result, neural networks possess the ability to learn intricate relationships between input and output data and find applications in diverse domains [59], though they are considered 'black boxes', meaning there are no methods for feature extraction from the model [60].

Deep learning is a sub-field of ML characterized by the use of deep NN, which involves the use of multiple hidden layers that can learn hierarchical representations of data. Deep learning models have proven to be particularly advantageous in EEG signal classification tasks, as they can learn complex features directly from raw data without the need for handcrafted features or preprocessing steps [3]. Moreover, these models can handle large datasets and high-dimensional inputs efficiently using shared weights and local connections. They can be trained end-to-end using gradient descent algorithms with backpropagation, which allows them to optimize the model parameters to minimize the classification error [57].

2.6.2 Convolutional Neural Network

CNNs are commonly used for classification tasks. They are usually built with three layers, with the convolutional layer being the most important one, hence its name.

The convolutional layer consists of a filter or a feature detector that is moved across the data while checking if that specific feature is present. The output is a feature map, which is a series of values that depict where in the data the feature is present. This process can be done multiple times by filters with different properties, allowing for more complex features to be found as the sum of its parts [61].

Following the convolutional layer is the pooling layer and the fully connected layer. The pooling layer reduces the risk of overly complex models by reducing the number of parameters. This makes for a more robust algorithm. Finally, the full-connected layer produces the output, translating from the similarity of features to an estimated match of category [62, 61].

Chapter 3

Literature Review

3.1 Current Communication Methods and BCIs for LIS

The communication techniques that are currently available for patients with BCIs are varied [63]. One common method involves alphabet boards in combination with blinking and eye movement to indicate letters. However, this method relies on the patient's caregiver having an active role in interpreting the movement in order to make out letters and convey the messages, which provides little to no privacy. Other techniques rely on innovative technology, such as eye-tracking, which while providing more independence, still requires a significant amount of time for communication [64]. This highly impacts social situations and affects the patients' opportunity to participate in conversations[9, 63]. Additionally, these methods might not be available if the patient is unable to move their eyes or blink voluntarily. For patients with CLIS, the only option may be BCIs that does not require any movement, but rather relies on other signals to be interpreted.

A study [65] that surveyed people with LIS on their preferred applications, mental strategies, and time of information for communication, found that they, in general, showed the same preferences. Scoring the highest on the application was direct personal communication, while the preferred mental strategy was attempted speech, followed by attempted movement. Incorporating the user group's involvement in the development of assistive technologies is crucial to ensure the utilization of optimal methods and the inclusion of necessary functionalities. By actively engaging the users throughout the development process, the resulting technologies can better address their specific needs and preferences. This user-centric approach helps to enhance the usability, effectiveness, and overall quality of the assistive technologies being developed.

There are already several types of BCIs that are being researched, some with promising reports. Implementing these technologies could improve patient care, increase patient engagement, and allow us to monitor the long-term impact of LIS on patients' health and quality of life [66]. Though devices for direct communication are a significant resource for this purpose, the field of use for BCIs is only growing. Allowing for easy computer access in time with the rise of smart homes could make more

tasks readily available, introducing a larger degree of independence [67].

The existing BCIs feature a wide range of paradigms and user requirements. For patients with CLIS, there exist several options under the category of invasive BCIs such as a spelling interface using intracortical signals [68] and a communication device using local field potentials[69]. These typically require implants or other direct connections to sensors under the skin, and while highly accurate, they also are expensive and might pose a risk to the patients' health. For patients in classical LIS, or patients retaining some motor control, the opportunities for stimuli change, and with them, the paradigms for BCIs. A study [70], found promising results using SSVEPs recorded over the visual cortex, supporting the possibility of utilizing visual stimuli. It also allows for mimicking the existing practiced methods for communication, leaving less new learning for both caregivers and patients.

Among the most popular non-invasive BCIs are the EEG-based systems [66]. The technologies that have emerged includes spelling devices [71, 72, 73], controllable wheelchairs [74, 75, 76], speech generators [77, 78] and control of humanoid robots [79, 80, 81]. Despite these achievements, it has been observed that many of the publications do not provide details on how EEG artifacts were managed [82]. This poses a significant problem as they not only contaminate the desired control signal but may overpower the classifier's detected features and create an undesired paradigm.

3.2 State-of-the-art in OA Removal

It is crucial to remove the artifacts that interfere with signal analysis in order to use BCIs for reliable communication. While effective methods exist, such as ICA, spatial filtering, and regression-based techniques [83], they typically require offline processing, which is slow and computationally intensive. Though these methods perform well at preserving the signal without distortion, they are not suitable for real-time applications like BCIs.

In a previous study [84], a real-time OA removal method was introduced, combining ICA with a Kalman filter. This method demonstrated promising outcomes by effectively removing OAs from EEG signals while minimizing distortion. The proposed method achieved a high detection rate of 98.4% for eye blinks, accurately identifying the occurrences of OAs. The removal process successfully eliminated the ocular noise without adversely affecting the alpha band, which is a frequency range of particular interest in EEG analysis.

Wavelet transform-based decomposition and selective removal of OA-associated frequency components are among the methods being researched for this use case [85]. These techniques have shown promise in achieving fast analysis and providing usable real-time processing for BCIs across a range of frequencies. To preserve the signal outside OAs, it is recommended to perform the removal algorithm only during short periods when necessary. In another study [47], a combination of artifact detection and removal was proposed to address this issue. The detection method involved using algebraic spike detection to identify segments likely to be OAs. This method achieved positive results in both artifact removal and real-time computing.

3.3 Previous Contributions to the Project

Two earlier works have been conducted as contributions to this project, namely a specialization project [11] and a master thesis [5]. The main objective was to investigate the potential of combining the brain's color perception and the user's eye movements to develop a straightforward communication system suitable for individuals with LIS. For this purpose, a dataset was collected using a protocol that displayed color on a screen, mimicking a possible protocol for the intended BCI. The four colors red, green, blue, and yellow were shown in intervals, interrupted by a black screen. This resulted in two types of tests: Classification of the four colors, as well as differentiation between a color and the black screen. Testing was done with a pipeline of preprocessing, feature extraction, and several classification techniques, including Random Forest (RF), Support Vector Machine (SVM), and CNN.

The results achieved accuracies of 69.87% and 73.6% for differentiating between task and rest states, and the four colors, respectively. This was concluded to be promising for the feasibility of the BCI. It was reported that one of the weaknesses in the dataset was the contamination of the rest state sample by eye blinks in order to preserve the samples of the four colors, which might contribute to the difference in result between the two experiments [5]. This speaks in favor of testing the thesis on another dataset that might be less affected by OAs, as well as highlights the importance of a BCIs capacity to deal with issues related to real-time use, such as eye blinks.

In previous studies, the dataset utilized in this thesis has been subjected to RGB classification using two different approaches: the Minimum Distance to Mean with geodesic filtering (FgMDM) Riemannian classifier [4] and a CNN model [86]. For the FgMDM Riemannian classifier, the preprocessing phase involved discarding epochs that contained artifacts, resulting in the classification being performed on artifact-free epochs. The average accuracy achieved using this classifier was 74.48% over a subset of subjects. In the case of the CNN classification, a hybrid method was employed. The OAs with the highest amplitude were discarded, while the OAs that had a lesser impact on the signal were removed using SSP (a technique called artifact removal using SSP). The classification results showed an average accuracy of 77% across all subjects and 84% for the same subjects as the FgMDM Riemannian classifier.

In this project, the same dataset is being utilized; however, a different focus is placed on artifact removal methods. The objective is to investigate whether it is possible to perform artifact removal effectively without the need to discard epochs, as discarding epochs is not feasible in real-time applications. By applying artifact removal techniques, the project aims to enhance the quality of the data and improve the overall classification performance. The goal is to develop methods that can successfully remove artifacts while preserving the underlying relevant information in the epochs. This would allow for real-time applications where all available data can be utilized for classification, without the need for discarding epochs due to artifacts.

Chapter 4

Materials and Methods

4.1 Software Tools

The implementation of this project relied on *Python* and various other packages. *MNE* [87] was employed for general EEG data handling tasks such as data loading, filtering, sampling, and visualization. The artifact detection FIR filter was implemented using the Signal library from *SciPy* [88]. *MNE*'s preprocessing package was used to implement ICA and SSP. For artifact removal, *PyWavelet* [89] was utilized for DWT and inverse DWT, while *Numpy* [90] were mainly used for mathematical purposes. An implementation [91] of *EEGNet* using *Tensorflow*'s library *Keras* was used as a basis for this project.

4.2 Dataset

The dataset was recorded at the NeuroImaging facilities of Aalto University in Helsinki [4]. The recordings took place in a high-end, three-layered magnetically shielded room where EEG recordings were taken simultaneously with Magnetoencephalography (MEG) measurements recorded by the MEG Core.

This project only has use for the EEG data, which were recorded using a 64-channel cap from antNeruo with a sampling frequency of 1000.00 Hz. A total of 60 electrodes collected EEG signals, while the other 4 were used as EOG channels in order to capture ocular and muscular interference. The EEG channel electrodes were placed after the international 10-20 system.

In total 31 subjects were recorded. For subjects 1-18 as well as for subject 26, the two channels 'Oz' and 'O2' were flat and therefore marked as bad. Some of these subjects were later re-recorded and therefore have 2 sessions, while the rest only have 1.

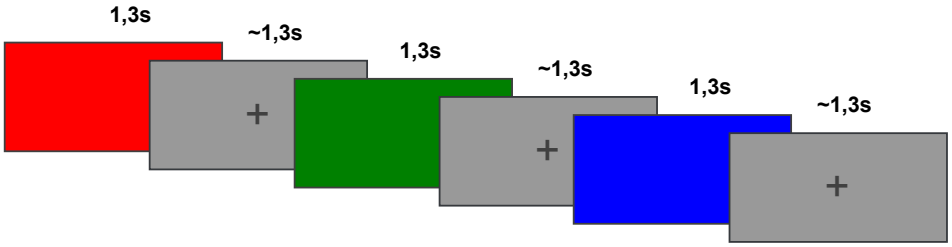

Figure 4.1: An illustration of the protocol used for collecting the data.

4.2.1 Protocol

The protocol consisted of the participants being placed in front of a screen and shown colors in intervals. The colors were shown in random order and with a gray screen between each color. A cross was added to the middle of the gray screen in order to let the participants rest their gaze. For the colors, the duration was set at 1.3s while the gray pause screen had a slight randomization between 1.3s and 1.6s in order to prevent the participants from getting used to the rhythm. The RGB color codes utilizes were FF0000, 008000, and 0000FF. An illustration of the protocol with duration and colors is shown in fig. 4.1. A total of 140 epochs of each color was recorded, with 4 pauses of 1 minute placed throughout to let the participants rest.

During the experiment, participants were instructed to avoid blinking the colored screen which implies that the epochs containing OAs are expected to be more prevalent during the gray screen, meaning the rest state. Additionally, a camera was utilized to capture video footage of the participants, allowing for the measurement of their engagement levels. It is worth mentioning that a few participants displayed signs of drowsiness and even fell asleep during the recording sessions.

4.2.2 Data Selection

The final data selection consists of sessions where all channels were reported as good and the participants were reported as awake and focused. The final data selection can be seen in table 4.1 with the final number of epochs in each class per session.

The presence of gray pauses inserted between each color screen ensures an equal number of data segments for both the gray screens and the combined total of the colored screens. This balanced distribution of data segments between the rest and task classes is crucial when attempting to classify these two classes.

Subject	Session	Rest epochs	Task epochs
2	2	425	420
3	2	424	420
4	2	425	420
5	2	425	421
6	2	425	420
7	2	425	420
8	2	425	420
11	2	425	420
13	2	425	420
14	2	425	421
15	2	424	420
18	2	425	420
19	1	425	420
20	1	425	420
21	1	425	420
23	1	422	420
24	1	425	420
25	1	425	420
26	2	425	420
28	1	425	420
29	1	425	420
30	1	425	420
31	1	425	420
Total		9770	9662

Table 4.1: Subjects and session with their total number of epochs used for the OA removal and subsequent classification

4.3 Preprocessing

Removing Powerline Noise

Electrical power lines produce a 50 Hz AC signal that can contaminate EEG recordings. To remove this noise, a notch filter was applied to remove the 50 Hz frequency component from the data.

Bandpass Filter

A bandpass filter was applied to the data to limit the frequency range of interest. Since frequencies in the gamma range are rarely encountered in EEG data, this range was chosen to be between 0.1 and 45 Hz. This ensures that any noise or artifacts that may have been introduced during data acquisition are removed.

Downsampling

The original data recording was done with a sampling frequency of 1000 Hz. Since the intended application of this is a BCI, it is beneficial that the signal processing and the classification using the NN can be completed in a real-time perspective. EEG signals have a high dimensionality and processing is computationally intensive, especially with a high sampling frequency. Additionally, higher frequencies require more processing power and storage capacity, making the equipment heavier and bulkier, which can be undesirable for everyday use where comfort and portability are important factors to consider. Therefore, downsampling the EEG signals can make the system more lightweight and comfortable, which is beneficial for practical applications. Based on this, downsampling to 200 Hz was applied to the signal.

4.4 Data Processing

After preprocessing the data, it was cleaned using the four methods presented in this section. All methods have the intention of removing ocular artifacts, specifically blinks as they are the most disruptive to the signal, while preserving the information in the recording. While ICA and SSP were implemented as well-established methods, the implementations of the modified SSP and the algebraic method were developed in this thesis.

4.4.1 Algebraic Method

The algebraic method used in this work was suggested by [47]. It is a hybrid algorithm that detects and removes the OAs. First, the algorithm detects OA zones based on algebraic calculation. Second, it removes the blinks by using DWT decomposition and thresholding. In contrast to the other methods used, the denoising is only applied to the area detected as an artifact. This results in a fast denoising technique, well suited for real-time applications, like BCIs.

In the original paper proposing the method, the decision function, eq. (2.3), was compared to the threshold

$$\gamma = \frac{N}{\mu + \sigma}, \tag{4.1}$$

where N is a constant found through experimentation, and μ and σ are the mean and Standard Deviation (SD), respectively. The value should be set so that the method detects sufficiently accurately on data from different subjects [47].

In [1, 2], it was found that some of the detected areas did not cover the complete spike in the signal. Experimentation was done to circumvent this. It was found that implementing padding to the detected areas on both sides of the region improved the detection, and was hence included in the algorithm.

After the detection of OAs, denoising using DWT with 8 levels of decomposition was applied to the detected regions. The frequency bands for 8 levels of decomposition using data with a sampling frequency of 200 Hz are presented in table 4.2. For each level, the DWT generates detail coefficients. To remove unwanted frequency components, coefficients exceeding a certain threshold are replaced with zero.

Level	Frequency band
D1	50-100
D2	25-50
D3	12.5-25
D4	6.3-12.5
D5	3.1-6.3
D6	1.6-3.1
D7	0.8-1.6
D8	0.4-0.8
A8	0-0.4

Table 4.2: The frequency bands corresponding to each detail coefficients obtained from a DWT with 8 levels of a signal with sampling frequency 200 Hz. Di denotes the detail coefficient at the i^{th} level and A8 is the approximation coefficient.

As discussed in section 2.3.4, OAs occur at low frequencies, but there are different reports as to the specific ranges that are relevant. For this project, 0-13 Hz will be used as this is also what was reasoned in the original article for the algebraic method [47]. By using levels 4 to 8 (corresponding to the frequency range 0.4-12.5 Hz) for denoising, the unwanted large contributions to the detail coefficients in this frequency range could be filtered out. After thresholding, inverse DWT was used to reconstruct the signal, and the original signal was exchanged with the reconstructed signal in the detected OA zones.

The mother wavelet was selected experimentally by testing different options such as 'coif5', 'bior4.4', 'sym3', and 'haar'. To determine the threshold for coefficient selection, three metrics were tested: Universal Threshold (UT), SD, and Median Absolute Deviation (MAD). The UT threshold was calculated using equations

$$T_{UT} = \sqrt{2\log N}\sigma \tag{4.2}$$

$$\sigma^2 = \text{median}\left(\frac{|C_a|}{0.6745}\right), \tag{4.3}$$

where N is the length of the data and C_a represents the wavelet coefficients at the a-th level. and 0.6745 is the constant value for Gaussian noise. The SD threshold was set to

$$T_{SD} = 1.5std(C_a) \tag{4.4}$$

as proposed by [92], where std is the SD of the a^{th} level coefficients. Similarly, the threshold based on MAD is

$$T_{MAD} = 1.5MAD(C_a) \tag{4.5}$$

In all cases, thresholding was applied to the absolute value of the coefficients using the `threshold` function from the PyWavelets library in 'less' mode, with a substitute value of zero.

Through experimentation, it was found that the 'bior4.4' wavelet combined with the UT gave the best results, and therefore the parameters chosen for this project.

4.4.2 Signal-Space Projection

The second OA-removal method used was SSP. The EOG channel was used to calculate the projection. First, an average EOG epoch was computed using the `create_eog_epochs` function from *MNE* preprocessing library. This function utilizes an EOG channel to extract epochs centered around the peaks of OA events. The threshold to trigger detection of such an event is based on the range of the signal. The average of these epochs is then used to estimate the spatial distribution of the EOG artifacts. The `compute_proj_eog` function was then used to calculate the projection vectors based on the spatial distribution. The resulting projection matrix was applied to the EEG data using the `apply_proj` function from *MNE*, which subtracts the projection from the EEG data to remove the EOG artifacts.

4.4.3 Signal-Space Projection - Modified Version

The third method used in this work is referred to as a modified version as it is a modification of how SSP is normally applied. As this work aims to find a denoising technique suitable for real-time applications, it is advantageous to reduce the calibration time needed for use.

Instead of using the whole session to find the best examples of the artifacts, only a small part of the recording was utilized. During the sessions, the participants had a pause of 1 minute so that the recording process was not too hard on their focus. At the time of the pause, the participants were not requested to look at the screen, but rather take a break, adjust their seating, and regain focus. This means that during this minute there exists OA such as blinks and eye movement, as well as possible muscle artifacts. Using only one of these minutes for calculating the SSP would make for a method that is both robust and requires little effort for calibration.

The continuous signal of one of the minutes was used along with the `compute_proj_eog` function to calculate the projection. This projection was then applied to the whole signal using the same method as described above.

The alternative approach is proposed as a more real-time suited OA-removal algorithm, more targeted towards BCI applications. The idea is that the user is asked to wear the EEG recording device and perform a brief calibration process by blinking for a short period of time. This calibration data is then used to calculate the projection matrix that can remove eye blink artifacts in real time during the subsequent use of the BCI system. This approach can potentially reduce the time required for preprocessing EEG data significantly, and possibly improve the accuracy of the BCI system since it is calibrated specifically for the individual user.

4.4.4 Independent Component Analysis

ICA is one of the most used methods in OA removal today, though it is computationally heavy and therefore not suited for real-time use or BCIs. It is, however, a good source for comparison of the performance of the other methods and provides a standard for how the results should look.

ICA was used to remove ocular artifacts from the EEG data using the `ICA` function from the preprocessing library of *MNE*. First, a high-pass filter with a cutoff frequency of 1 Hz was applied to remove slow drifts and other low-frequency noise. The filtered data were then used as input to the ICA algorithm. Secondly, the `ICA` function performs independent component analysis on the input data. The number of components to estimate was set to 20 and automatic regulation of the maximum number of iterations was used.

To identify components related to eye movements, the `find_bads_eog` function in *MNE* was used. This function automatically detects ICA components that are correlated with the EOG data, which is a direct measure of eye movements. The function returns the indices and scores of the components that are most strongly correlated with the EOG. These components can then be excluded from the ICA decomposition by setting the `exclude` attribute of the `ICA` object.

Finally, ICA was applied to the preprocessed data to remove the ocular artifacts. The `apply` method of the `ICA` object was used to project the EEG data onto the ICA components and then back-transform to obtain the denoised data.

4.5 Classification

This section details the choices made for the classification tasks. In order to assess differences in the performance made by the process of color perception in the brain, tests were done on both the whole set of channels, and a subset more closely associated with the relevant regions, namely the six channels 'PO3', 'POz', 'PO4', 'O1', 'Oz', and 'O2'. For all tests, the same implementation was utilized.

4.5.1 EEGNet

The classification will be done by *EEGNet*, a compact CNN that has been developed for EEG use. NN usually demand being specially built for the specific use case, while this open-source model aims to work as a generalized CNN that can work across different paradigms. This makes it highly relevant for this project as its focus is not on building the best classifier, but rather comparing methods in signal

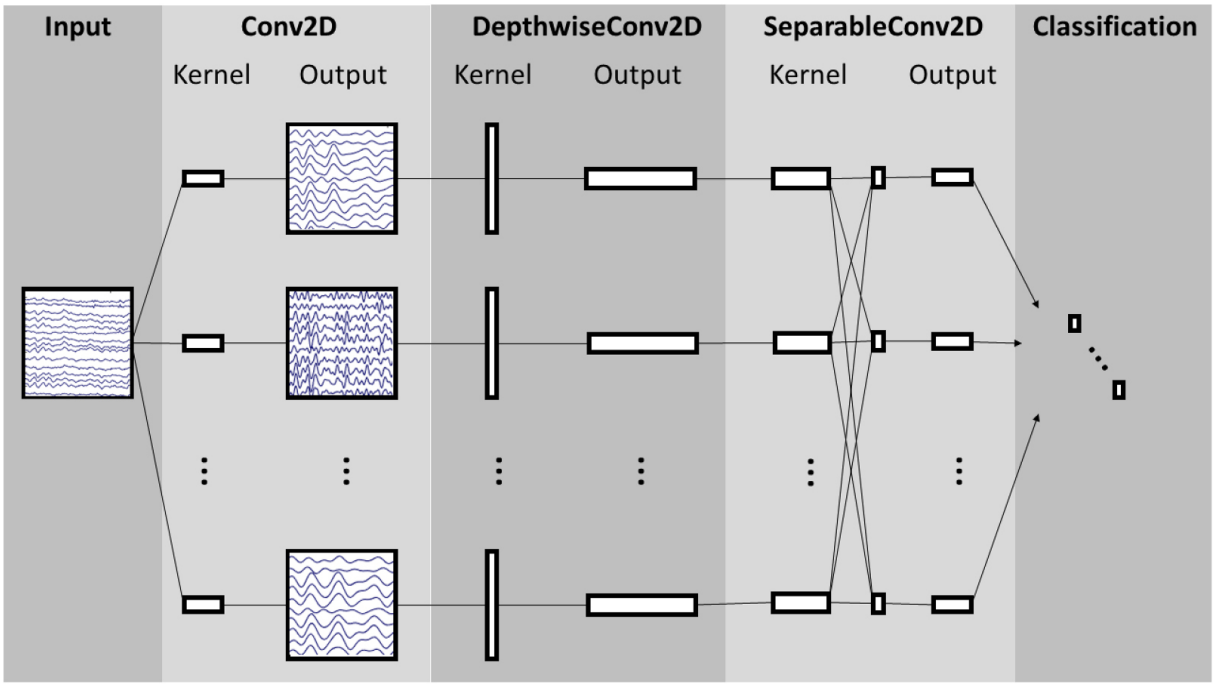

Figure 4.2: A visualization of the structure of *EEGNet*. Reprinted from [3]

processing.

The network consists of three main components: a depthwise temporal convolution layer, a separable spatial convolution layer, and a depthwise temporal convolution layer with stride. These are all visualized in fig. 4.2. The first temporal convolution layer operates on the time axis of the input data, while the spatial convolution layer operates on the electrode axis. The second temporal convolution layer with stride reduces the temporal resolution of the output and enables the network to learn high-level temporal and spatial features.

More details on the parameters of the model are depicted in table 4.3. Parameters F_1 and D are the number of temporal and spatial filters, respectively. F_2 is a hyperparameter that sets the number of feature maps.

4.5.2 Implementation of *EEGNet*

The implementation was adapted from the provided example at [91] in order to accommodate the data sampled at 200 Hz, which deviates from the example implementation intended for 128 Hz data. The kernel length, which is typically set to half of the sampling rate in *EEGNet*, was adjusted accordingly to 100 Hz instead of 64 Hz. This modification was made to ensure that the *EEGNet* model can effectively process the data and capture the relevant temporal features. This adjustment was the only modification made to *EEGNet* for this specific project.

Block	Layer	# filters	Size	# params	Output	Activation	Options
1	Input				(C, T)		
	Reshape				(1, C, T)		
	Conv2D	F1	(1, 64)	64 · F1	(F1, C, T)	Linear	Mode = same
	BatchNorm			2 · F1	(F1, C, T)		
	DepthwiseConv2D	D · F1	(C, 1)	C · D · F1	(D · F1, 1, T)	Linear	Mode = valid, depth = D, max norm = 1
	BatchNorm			2 · D · F1	(D · F1, 1, T)		
	Activation				(D · F1, 1, T)	ELU	
	AveragePool2D		(1, 4)		(D · F1, 1, T // 4)		
	Dropout				(D · F1, 1, T // 4)		p = 0.25 or p = 0.5
2	SeparableConv2D	F2	(1, 16)	$16 \cdot D \cdot F_1 + F_2 \cdot (D \cdot F_1)$	(F2, 1, T // 4)	Linear	Mode = same
	BatchNorm			2 · F2	(F2, 1, T // 4)		
	Activation				(F2, 1, T // 4)	ELU	
	AveragePool2D		(1, 8)		(F2, 1, T // 32)		
	Dropout				(F2, 1, T // 32)		p = 0.25 or p = 0.5
	Flatten				(F2 · (T // 32))		
Classifier	Dense	N · (F2 · T // 32)			N	Softmax	Max norm0.25

Table 4.3: The *EEGNet* architecture, reprinted from [3], is defined by the following parameters: C represents the number of channels, T is the number of time points, $F1$ is the number of temporal filters, D represents the depth multiplier (number of spatial filters), while $F2$is the number of pointwise filters, and N is the number of classes.

4.5.3 Data Processing for Classification

Reference Electrode

The EEG data was recorded without using a reference node. Therefore, a virtual reference was applied using common average referencing across all the channels, to estimate the signal at the virtual reference.

Epochs

To isolate event-related activity in EEG signals, the data was divided into epochs of 1.45 seconds, containing 291 samples. This approach enabled the classification of patterns of brain activity that corresponded to specific cognitive processes or events. Each epoch included a baseline period of 0.2 seconds before the event onset and a post-stimulus period of 1.25 seconds. The baseline period captured the brain activity before the cognitive event, while the post-stimulus period captured subsequent activity associated with the event. Including both periods allowed better isolation and analysis of the event-related activity in the EEG signals by including the onset of the event. Additionally, including the baseline period accounted for individual differences in baseline brain activity and ensured that the classification was based on relative changes in activity associated with the cognitive event.

Epoch Rejection

Normally, epochs that have a peak-to-peak amplitude larger than $150\mu V$ would be rejected as a means to avoid parts of the signal that are polluted by muscle signals, environmental noise, or electrode artifacts. However, as the aim of this project is to investigate OAs, this step was left out of the signal processing. This way, all the methods had the same basis for training and testing the classifier. The total number of epochs for the rest and task states can be seen in table 4.1 and shows that the

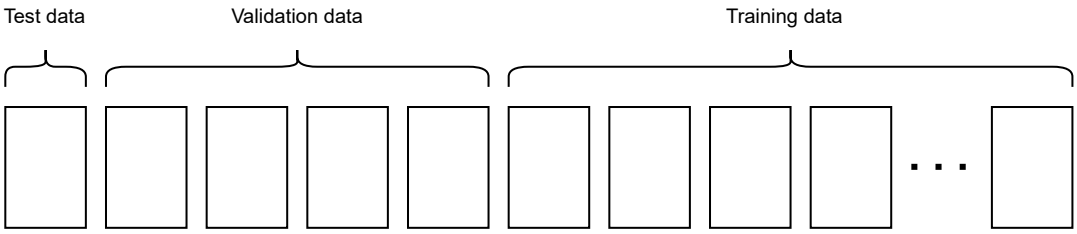

Figure 4.3: Illustration of the training, validation, and test sets. Each rectangle represents a recorded session from a subject.

dataset is approximately balanced between the two classes.

Training, Validation, and Test Data

In ML, Leave-one-out Model (LOOM) refers to a technique where, during model evaluation, each data point in the dataset is used as a separate test sample while the remaining data points are used for training the model. This means that for a dataset with N samples, N different models are trained and evaluated, where each model is trained on N-1 samples and tested on the left-out sample.

For this project, this segmentation was implemented using each subject as a separate test sample, as illustrated in fig. 4.3. One subject was set aside, while the rest were randomized and split into a training set and a validation set by a ratio of 80-20, rounding up to 18 and 4 subjects, respectively.

4.6 Pipeline

The final pipeline for the signal processing is presented in fig. 4.4. The dataset underwent five distinct processing approaches, which in turn served as training data for five distinct NN models. Among the datasets, four underwent OA removal in addition to preprocessing, while the fifth dataset was exclusively applied preprocessing without any OA removal.

4.7 Metrics for Evaluation

In this section, the metrics that will be used to evaluate the effectiveness and performance of the methodology will be discussed. The evaluation of the OA removal will first be done visually to the extent possible. However, the evaluation will also be complemented by the accuracy achieved through the classification of NN models. This combined approach allows for a comprehensive gauge of the efficiency of OA removal and its influence on the overall performance of our methodology.

4.7.1 Evaluation of OA Removal

For an EEG signal in real-time, there exists no noiseless signal for comparison. As such, the evaluation of the effectiveness of the OA removal cannot be based on a direct comparison with the true target value. If this were to be the case, the OAs would have to be made by inserting artificial peaks that were

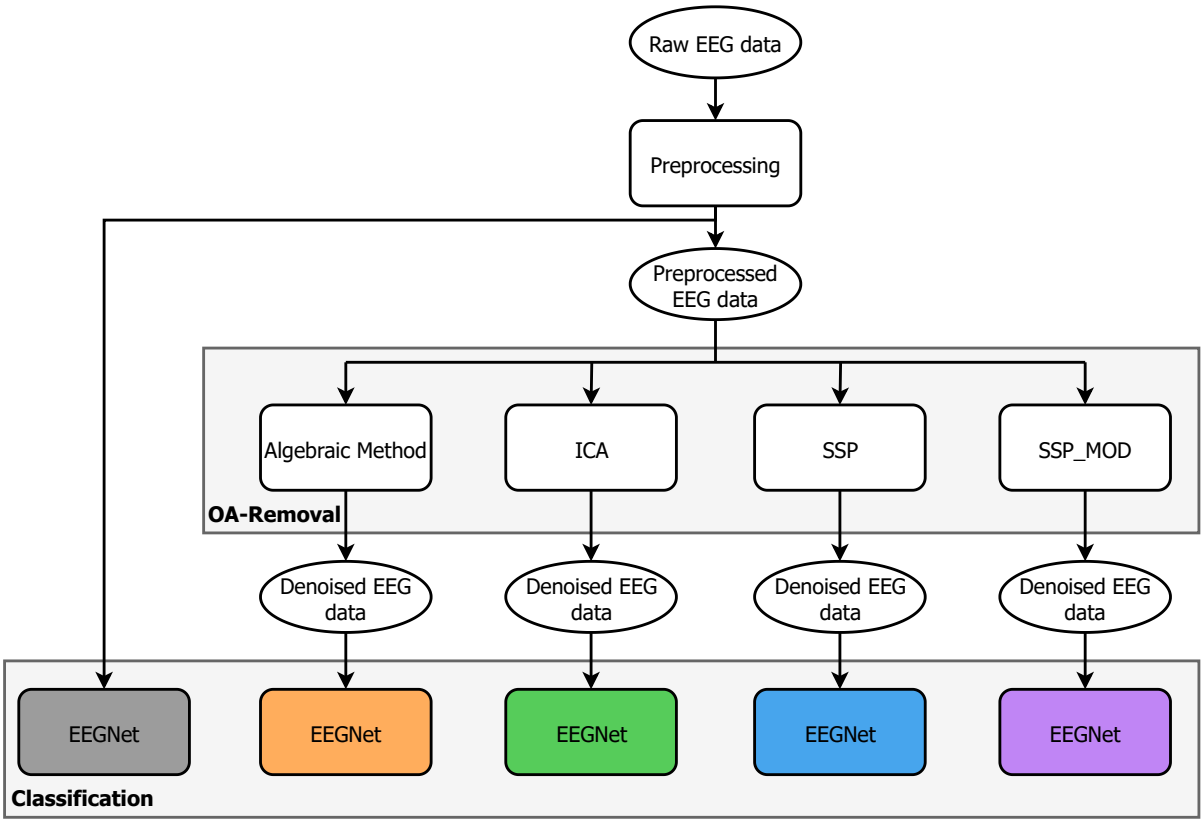

Figure 4.4: The intended processing pipeline for this project. EEG data is applied the same preprocessing and then four methods of OA de-noising. The resulting data is used to train and test four neural networks.

similar to the ones detected in the data. For this project, however, the analysis will be done on data containing real OAs.

Coherence

For the results of the data processing, a coherence plot will be employed. Coherence is a measure that describes the degree of similarity between two signals as a function of the frequency. The blink artifacts occur in a specific frequency range that the removal processes used should eliminate. If the processes are executed correctly, there should be low coherence within the specified OA frequency range (0-13 Hz), and a higher coherence value for frequencies outside this range. Ideally, only the specified frequency range should be affected, and since the algebraic method only targets these frequencies this is likely the outcome of this method. However, since both ICA and SSP also are used for general noise removal, it is likely that other frequency ranges will be affected as well.

Furthermore, the coherence plot provides additional information about the overall performance across all channels in the data, allowing for an understanding of the effects of the different denoising tech-

niques across the entire EEG recording. By examining the coherence values for each channel, channels that may require further processing or investigation to improve the overall signal quality can be identified. It is worth noting that while the coherence plot provides valuable information about the degree of similarity between two signals, it should not be interpreted as a direct measure of the effectiveness of removing OAs.

Visual Inspection

Given that there are no means of quantitatively assessing the effectiveness of the OAs removal process in separating the OAs from the underlying neuronal activity, a subjective assessment is required. Specifically, a visual inspection should be performed on the processed signal to evaluate the extent to which it resembles a typical EEG signal and to identify any potential artifacts that may have been introduced during the denoising process. This subjective evaluation provides an important way of assessing the quality of the denoised signal and can help to ensure that the removal of OAs does not compromise the underlying neuronal activity.

4.7.2 Evaluation of Classification

To evaluate the four CNN models generated by the four differently denoised datasets, and the preprocessed data, a confusion matrix will be employed. In a two-class classification, the matrix will be a 2×2 matrix, on the form shown in table 4.4, where the diagonal presents the number of correctly classified samples, while the other elements are the number of incorrect classifications. For each class, statistical metrics can be calculated for further insight into the performance. The one used in this work will be accuracy, which is defined as

$$Accuracy = \frac{TP + TN}{TP + TN + FP + FN}, \tag{4.6}$$

where TP is the number of true positives, TN is the number of true negatives, FP is the number of false positives, and FN is the number of false negatives. The optimal value is 1, which would mean that all predictions were correct. Other metrics might highlight the classification results if the dataset was unbalanced. However, since this is not the case for this project, accuracy is the only metric that will be considered.

		Predicted	
		Positive	Negative
Actual	Positive	True Positive	False Negative
	Negative	False Positive	True Negative

Table 4.4: Illustration of a 2-class confusion matrix

To summarize the accuracies obtained per method, a box plot will be used. A box plot is a graphical representation of the distribution of a dataset. It provides a visual summary of key statistical measures, such as the median, quartiles, and potential outliers, as illustrated in fig. 4.5. The plot consists

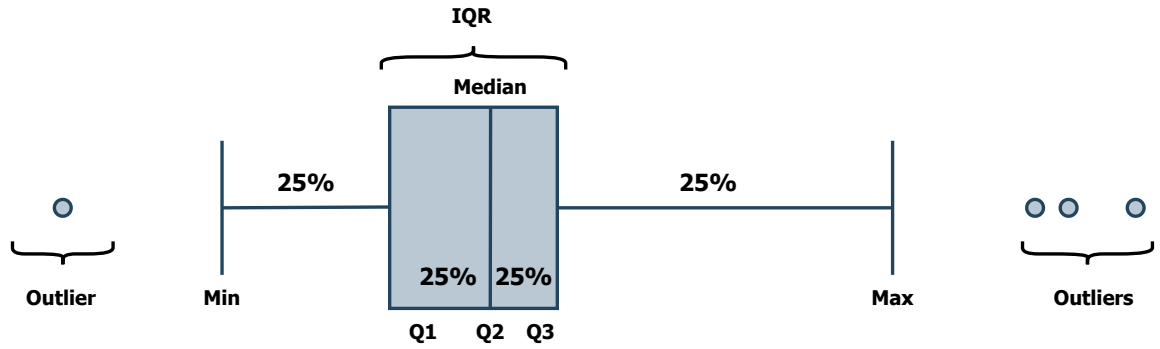

Figure 4.5: An illustration of a box plot. IQR is the interquartile range

of a rectangular box that represents the interquartile range, with a horizontal line inside denoting the median. Whiskers extend from the box to indicate the range of the data, excluding outliers, which are typically displayed as individual points beyond the whiskers. Box plots are useful for comparing distributions, identifying skewness or outliers, and understanding the spread and central tendency of a dataset.

Chapter 5

Results

5.1 Ocular Artifact Removal

The following experiments were done to analyze the performance of the removal techniques of the dataset. For all tests, the preprocessing was done as explained in section 4.6. The different removal techniques were then applied to the whole signal of each session.

To ensure simplicity and consistency, session 2 from subject 14 was deliberately chosen for the plots and figures presented in this section. The selection of this session was not random but intended to showcase the representative response observed in the EEG data. In addition to the processed signal samples, coherence plots were included as visual examples for inspection. Three specific channels, namely 'Fpz', 'Cz', and 'Oz', were selected for the coherence plots to highlight the variations in responses across the scalp.

5.1.1 Algebraic Method

The algebraic removal method was applied according to the method described in section 4.4. Analysis of the EEG data processed by the algebraic removal algorithm revealed that the detection of OAs varied depending on the electrode location. Figure 5.1 presents a section of the denoised processed signal compared to the original preprocessed signal. There is a noticeable difference between the amount of detected OAs in the three channels. Specifically, in the frontal electrode, only the most rapid spikes were detected, while in the central and occipital electrodes, all artifacts were detected. Additionally, multiple regions in the occipital lobe were identified as regions containing OAs, despite not actually being indicative of such.

In the comparison of the channel data in fig. 5.1, there is a notable distinction in the amplitude of the artifacts in the different channels. In the two more posterior channels, there is a larger amplitude of the spikes compared to the frontal channel. It is possible that the algorithm was unable to detect the lower amplitude artifacts. Additionally, the method has successfully detected blinks with similar amplitudes as those it failed to detect in 'Fpz', despite the more variable signal in 'Oz'. This suggests

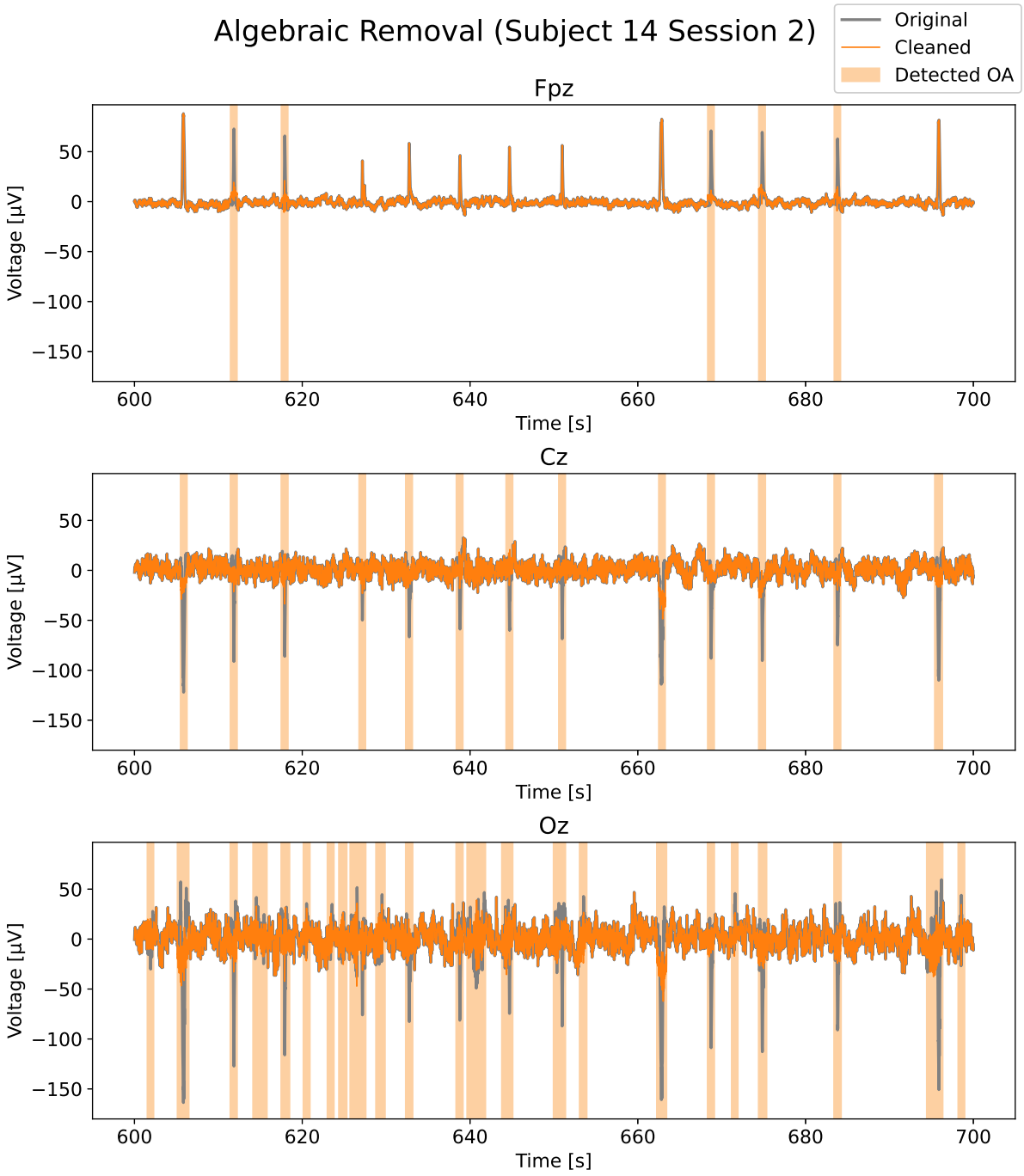

Figure 5.1: An example of the cleaned signal using the algebraic removal method compared to the original signal, for three of the channels from the second session of subject 14. The algebraic detection resulted in the OA-zones marked with the orange background in the figure. The method failed to detect some of the OAs in 'Fpz', and detected OAs at times no OAs were contaminating the signal in 'Oz'.

that the small amplitude alone is not the sole cause of the detection problem.

In fig. 5.1, it is evident that the SD of the signal increases in the posterior direction, resulting in a smaller spike-to-signal ratio. This smaller ratio should pose a higher challenge in distinguishing spikes in the posterior electrodes. However, since the algebraic detection method uses the inverse SD of the signal to scale the threshold, the threshold will decrease in the posterior direction, resulting in the observed over detection.

To illustrate some of the effects of the algebraic removal method and its effectiveness in reducing artifacts, a comparison of the signals of a single OA has been included, shown in fig. 5.2. This shorter time frame allows for a more detailed analysis of the results. The interval is chosen specifically to illustrate different occurrences that generally happened in the data. This detailed analysis is only presented for this specific removal method because the other three techniques do not have a separate detection algorithm, but rather use a transformation applied to the data as a whole.

The performance of the algebraic method is highly dependent on the detection performance. As seen in fig. 5.2, both the detection and the accuracy vary. The figure presents one OA, where the detection is significantly different in the three channels. In the frontal channel, 'Fpz', the OA is not detected at all, while in the central and occipital electrodes, it is detected. Although the OA is detected in both, the start time is substantially earlier in the occipital channel than in the central one. The detection determines the amount of the signal that is denoised with the removal algorithm. When applying DWT to the signal, thresholding the coefficients, and then reconstructing it with the inverse transformation, some information may be lost. For this reason, it is advantageous to have the algorithm minimize the duration of the identified OA interval, to the actual duration of the OA.

When evaluating the efficacy of the algorithm, it is observed that the method exhibits satisfactory performance in removing the detected OAs. The algorithm generally performs well in removing high-amplitude spikes while preserving the EEG signal's normal behavior, as far as a subjective visual assessment is concerned. However, some exceptions occur where some of the trend in the spike remains for certain large spikes. This is an indication of the threshold used for the detail coefficients in the DWT, was too high.

Occasionally, in the transition from the original signal to the denoised signal, a voltage drop is introduced. The phenomenon can be seen in the central electrode in fig. 5.2, at the start of the detected OA interval. When a voltage drop is introduced, some of the information in the original signal is lost. This can lead to a distortion of the signal, potentially making it more difficult to interpret the signal correctly, which could become apparent when using the resulting data in the classification.

As stated previously, the method sometimes detected an interval exceeding the actual OA. This is unfavorable, however, as seen in the occipital lobe in fig. 5.2, the majority of the EEG data is preserved at the beginning of the interval. This observation suggests that the method is capable of preserving the EEG signal's integrity to a significant degree, even when it is applied to an interval that extends beyond the actual duration of the artifact. The ability of the method to retain the EEG's normal be-

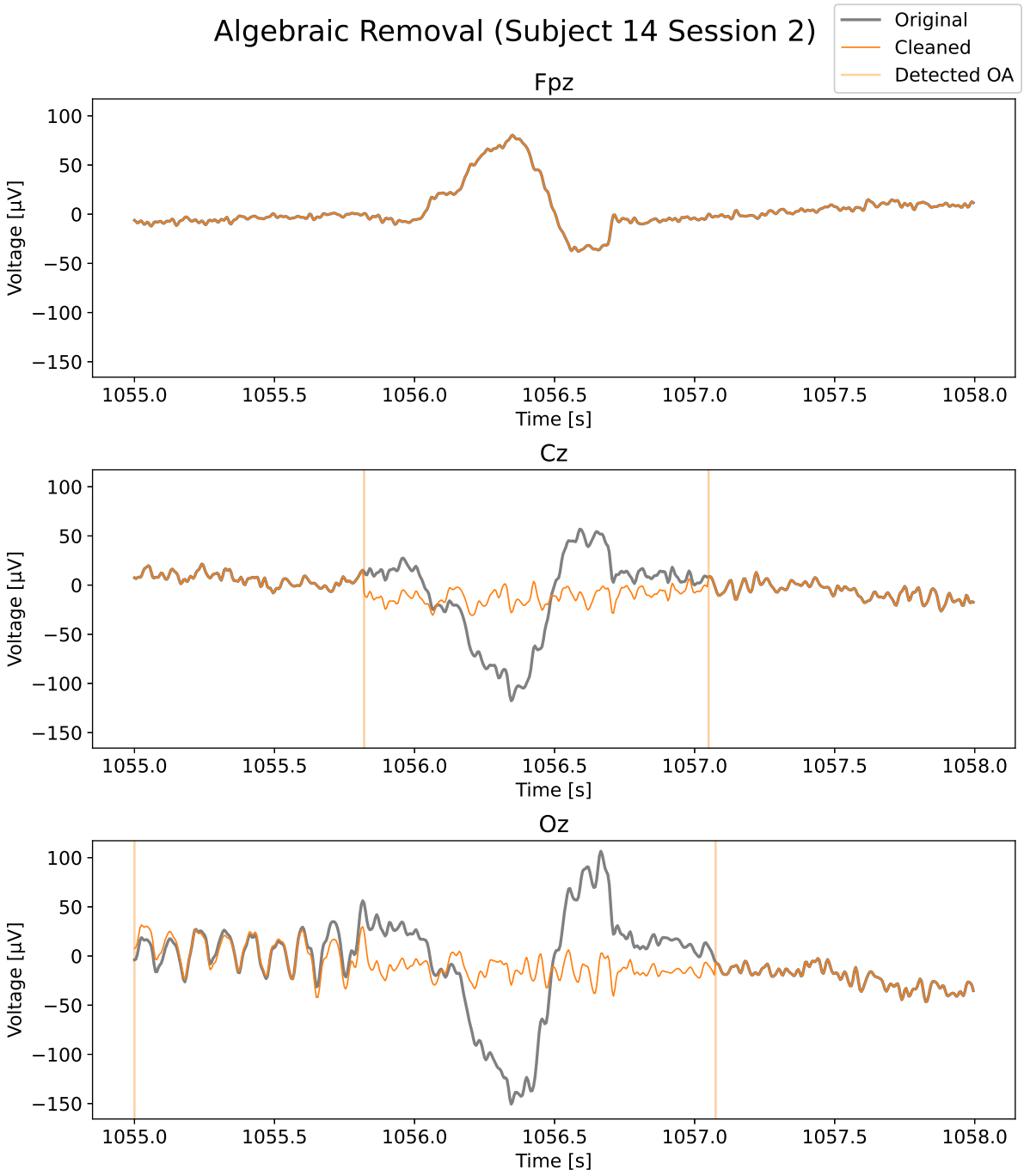

Figure 5.2: An example of a single OA from the second session of subject 14, comparing the cleaned signal using the algebraic removal method to the original signal. The detected OA zones are marked for each channel. 'Fpz' did not detect an OA zone and therefore the original and cleaned signals are the same for this example, while 'Oz' detected a larger zone than 'Cz'.

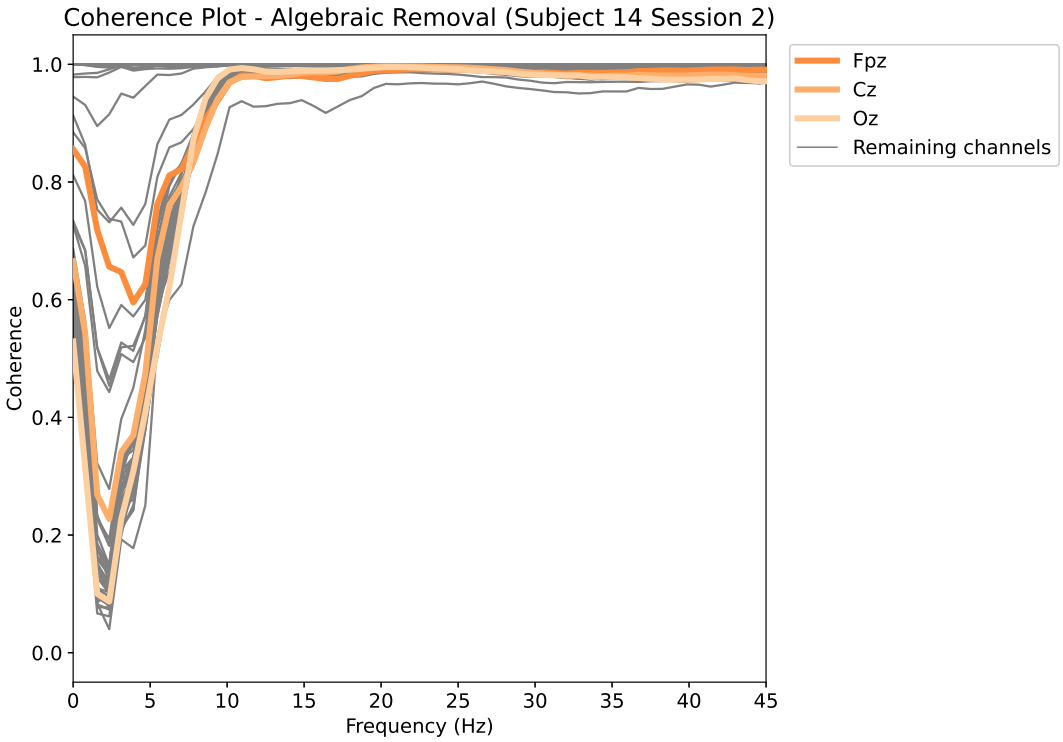

Figure 5.3: The coherence between the channel data from the second session of subject 14, before and after applying the algebraic removal method. Each line represents the coherence of one channel. Three of the channels are colored as shown in the legend to showcase the differences across the scalp.

havior for the majority of the interval suggests that the algorithm is not overly aggressive in removing non-artifact portions of the signal. Therefore, despite the occasional over-detection of artifact intervals, the method preserves a significant portion of the EEG data, which suggests that over-detection is not detrimental to the quality of the signal.

To gain more insight into the effects of the removal method, the coherence between the channel data of the original and the processed data was computed. Figure 5.3 presents the coherence, where each line represents the coherence between the original and processed channel data. The highlighted channels are the same as the ones discussed previously. As wanted, the coherence is close to one for high frequencies, while in the frequency band where OAs contaminate the data, the coherence is lower for the majority of the channels. The close coherence in the upper frequencies of likely highly contributed to by the fact that the original signal is still present in the areas where there was not detected any OAs. The frequency band of the detail coefficients being thresholded is 0.4-12.5 Hz, corresponding to the dip in the correlation. Some of the channels have a smaller dip in coherence. This could be caused by either there being fewer OAs in the channel data, or fewer being detected. As previously seen in fig. 5.1, there were fewer OAs being detected in the frontal electrode, which results in a smaller amount of the signal being processed, explaining the higher coherence. Contrarily, all spikes were detected in the central and occipital electrodes in fig. 5.1, causing a larger portion of the data to be denoised, causing a smaller similarity between the original and cleaned data.

Subject, session	2, 2	3, 2	4, 2	5, 2	6, 2	7, 2	8, 2	11, 2	13, 2	14, 2	15, 2	18, 2
No. of components	2	2	2	2	2	2	2	2	2	3	2	2

Subject, session	19, 1	20, 1	21, 1	23, 1	24, 1	25, 1	26, 2	28, 1	29, 1	30, 1	31, 1
No. of components	2	2	2	3	2	2	2	1	2	2	2

Table 5.1: The number of ICA components removed per session.

5.1.2 Independent Component Analysis

The ICA was done using the *MNE* library and was performed in multiple iterations in conjunction with a visual inspection, as is the norm. For each iteration, the components are chosen based on their similarity to the EOG and the scalp field topographies for each component. The effect on the EEG data was monitored and used in addition to the others to decide the final number of iterations, as well as the success of each iteration. For all the subjects the number of rounds was between 1 and 3, and for session 2 of subject 14, the number of iterations was 3. Table 5.1 shows the number of components removed for each session.

An example of the signal after the application of ICA for channels 'Fpz', 'Cz', and 'Oz' is shown in fig. 5.4. For all 3 channels, the artifacts were visibly reduced, as was the goal of the visual inspection during the removal process. The recomposed signal also appears to retain the overall shape and amplitude of the original signal, even where there was previously OA. However, when the two signals are overlapped as shown in the figure, it is clear that the ICA process has introduced some delay to the signal. This is due to the ICA object being fitted to FIR-filtered copy of the signal before being applied to the original. This can be offset by the baseline correction when dividing the signal into epochs for the classification.

How the effect of the ICA varies over the different channels can be discussed from the correlation plot of fig. 5.5. The same three channels have been highlighted in color. As the effect of the removal was apparent in fig. 5.4, it is to be expected that the frequency similarity to the original has been changed for these channels.

Generally, the curve of the lower frequencies matches for most of the channels. This result is consistent with the frequency range expected to be the source of the noise. For the frequencies above this range, the coherence is varied but generally follows the same pattern, meaning that there is a clear trend and common response for most of the channels. The variance could be due to the removal of other noise the ICA found with the OA, or indeed the opposite; linear noise introduced by ICA. Since the signal is decomposed into linear components, the subtraction of these components may also introduce noise or artifacts. Added rounds of ICA were found to further this behavior, as the components represented the artifacts less after each round.

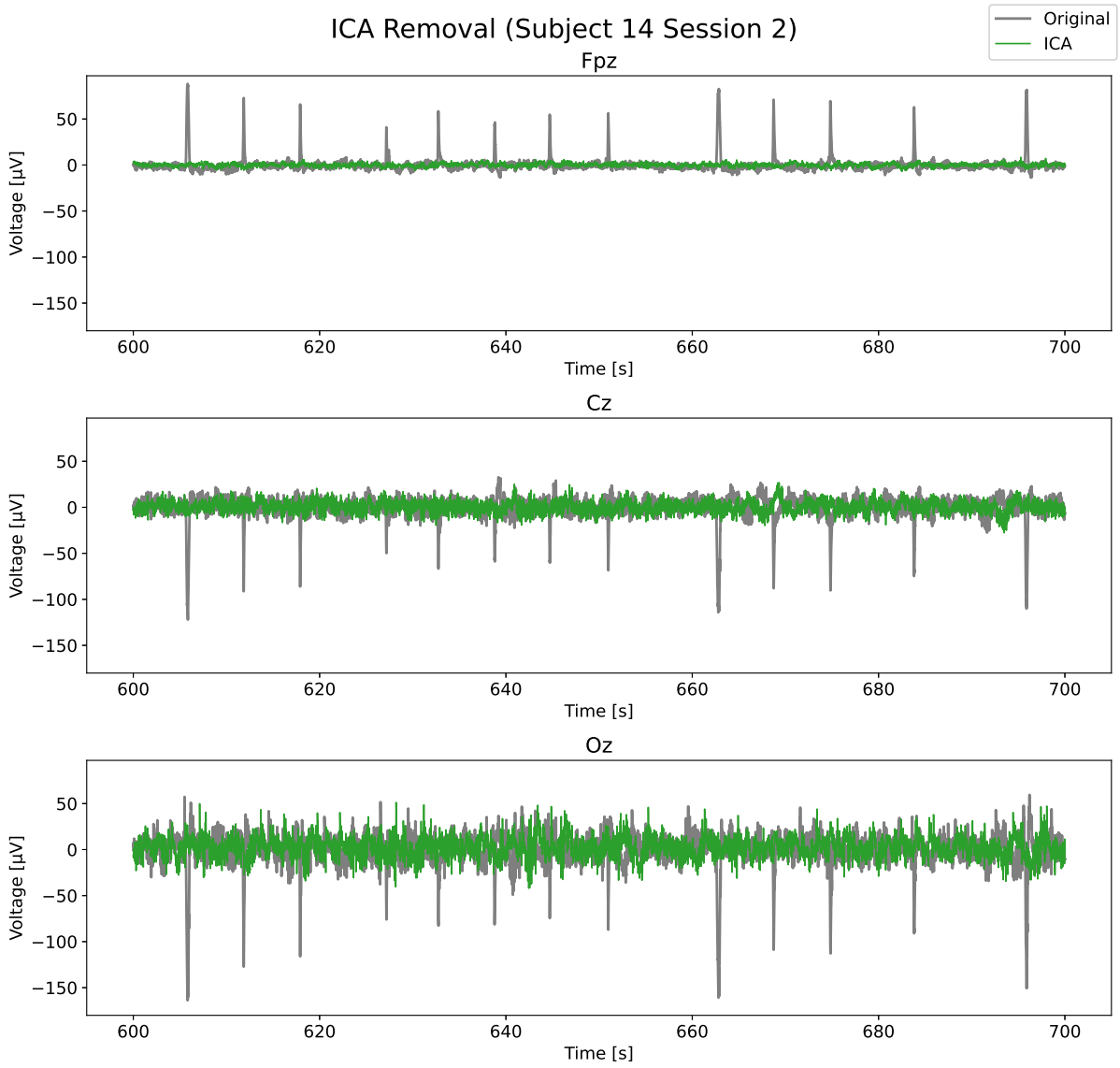

Figure 5.4: An example of the cleaned signal using ICA compared to the original signal for three channels from the second session of subject 14, over a period of time.

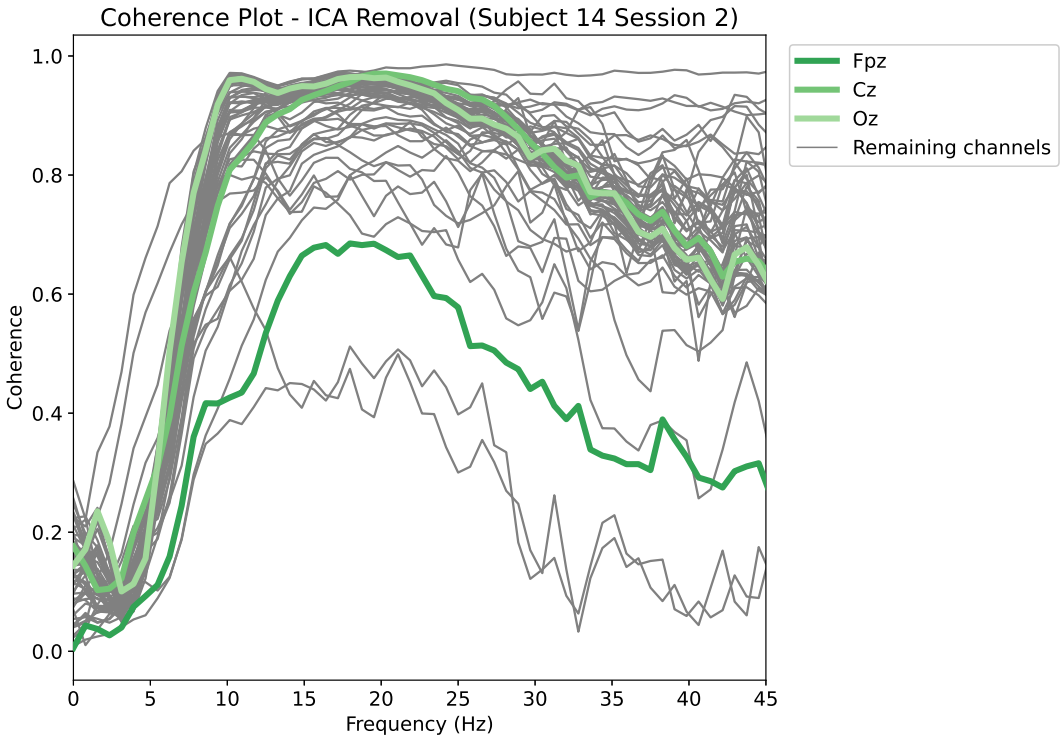

Figure 5.5: The coherence between the channel data from the second session of subject 14, before and after applying ICA for an example session. Each line represents the coherence of one channel. Three of the channels are colored as shown in the legend.

5.1.3 Signal-Space Projection

The SSP method was applied in two ways, as explained in section 4.6. After some experimentation over all the subjects, it was concluded that the number of vectors should be set to 1 for all. Adding more vectors did not make a visible impact, but rather added noise found in the coherence plots presented shortly.

Examples of the signal after the SSP and the modified version of SSP were applied are presented in fig. 5.6 and fig. 5.7, respectively. When comparing the two results, they both manage to project the signal to a subspace that captures all the artifacts. However, the method using the modified SSP exhibits some remnants of artifacts. While they both still display the same patterns as the original signal, fig. 5.7 seems to also carry the pattern of the artifacts, though still lowering the amplitude of the spikes. This modified SSP only used a sample of 60 seconds to calculate the subspace for the projection, while the other had the whole session. This means that the samples of characteristic artifacts to model the noise after were not equally distributed and were also likely contaminated by other OAs as well as muscle artifacts. The limited sample space could account for why the whole artifact was not removed by the modified SSP.

For channels 'Cz' and 'Oz' the signal amplitudes were significantly reduced in both methods, which may especially pose a problem if the artifacts are still present as this may affect the signal-to-noise ratio. In general, it means that modifications to the whole signal make visual inspection more de-

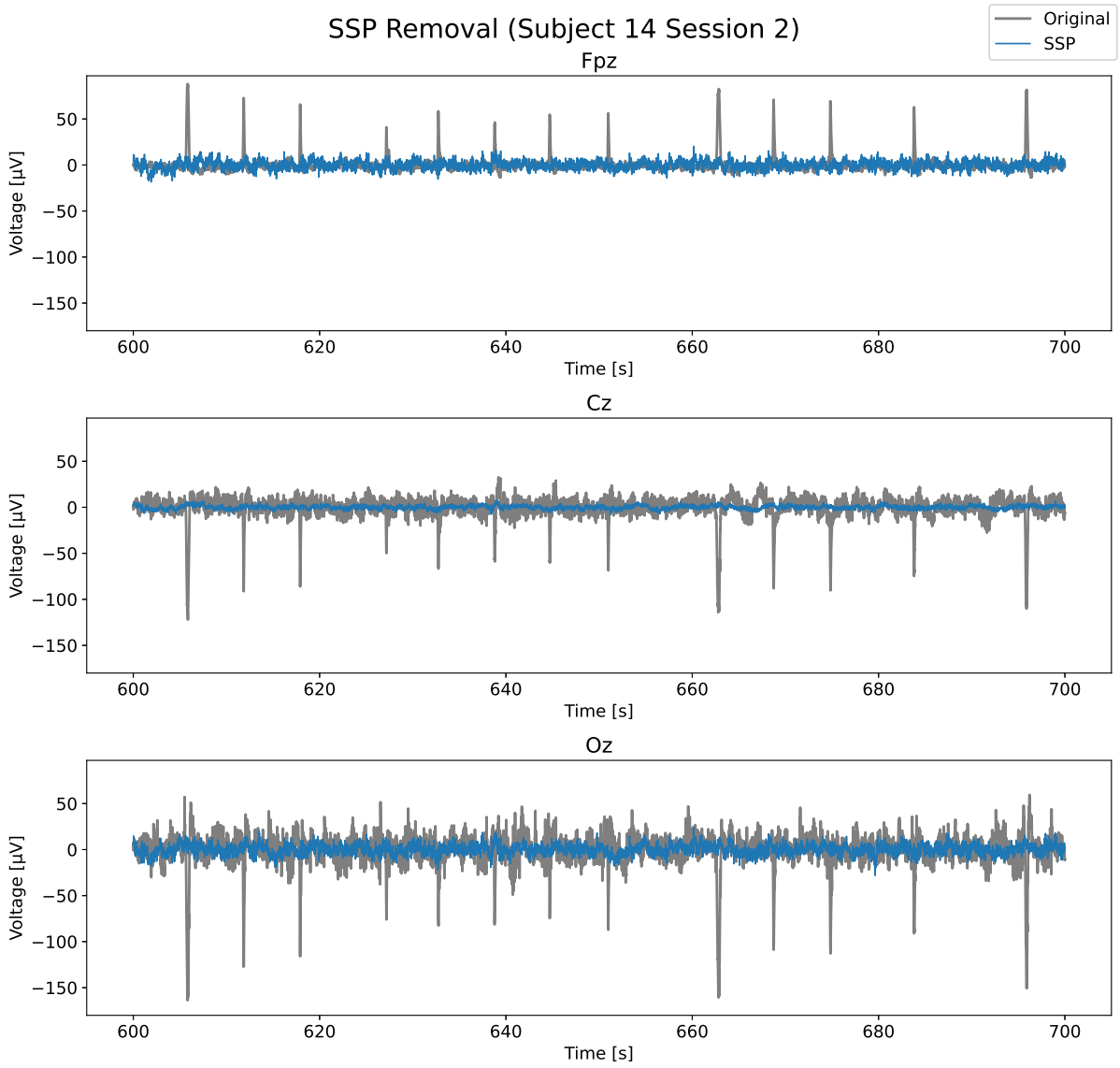

Figure 5.6: The cleaned signal using SSP compared to the original signal for three channels from the second session of subject 14, over a period of time.

Figure 5.7: The cleaned signal using the modified version of SSP compared to the original signal for three channels from the second session of subject 14, over a period of time.

manding and requires more than a simple comparison between the original and remodeled signals. The removal of a subspace from a signal introduces complexities in its interpretation, posing challenges to accurate understanding. By eliminating an inaccurate subspace, vital information related to the signal's underlying structure and relevant features may be lost, impeding accurate analysis and potentially leading to misinterpretations.

SSP is used under the assumption that the noise exists in a subspace that is orthogonal to the signal space. If this is not the case, there is a risk that parts of the desired signal may also be reduced. Looking at the coherence between the original recording and each of the signals produced by these two methods in fig. 5.8 and fig. 5.9 restates the difficulty of accurate interpretation of what noise the removal of the subspace might introduce to the signal, or what signal features may be lost. Most of the channels do exhibit a lower coherence for the frequency range associated with OAs. Even for the channels that still have quite a high coherence, there is a dip in the area 0-5 Hz, which speaks in favor of SSP as a tool for OA removal. For the higher frequencies, on the other hand, there is by comparison a lack of pattern and similarity across the channels.

For comparison of the two SSP methods, fig. 5.10 shows the coherence between them. Though the bottom part of the frequency spectrum shows some differences, it should be noted that they are all above 0.86. The fact that it is in this area that carries dissimilarity is quite to be expected following the comparison of fig. 5.6 and fig. 5.7. Provided that SSP is a satisfactory method for OA removal that preserves the desired signal, it stands to reason that the modified version also will perform well. As there is limited knowledge on this performance to be gathered from the example and coherence plot, this should be further evaluated by the performance of the classification algorithm.

5.1.4 Comparison of Performances

The algebraic removal method differs from the three others by only altering the data in the detected intervals. This makes the signal outside the OA-zones equal to the original, leaving the signal unaltered and preserving the information. Since the other methods are applied to the signal as a whole, there is no assurance of preserving the integrity of the information. As seen in fig. 5.11 at the end of the plotted interval in 'Cz', the algebraic method is equal to the original signal, as it is outside an OA-zone, while the signals processed with the three other methods diverge from the trend of the original signal. Conversely, the detection-limited OA removal approach, as exemplified by the frontal electrode in fig. 5.11, demonstrates that it may not successfully eliminate all OA artifacts. In contrast, methods such as SSP and ICA offer a distinct advantage in this regard. As projection-based and transformation-based techniques are applied to the entire signal, SSP and ICA have the capacity to capture and address a broader range of OA artifacts. This comprehensive approach ensures that OAs are not skipped, contributing to a more thorough removal of unwanted artifacts.

As verified by the coherence plot in fig. 5.10, the signals obtained from the two SSP methods exhibit a remarkable level of similarity, with virtually indistinguishable differences in fig. 5.11. It should be noted that this level of similarity was not as high throughout the whole dataset, however, overall the methods did produce remarkably similar results. The observed level of similarity between the signals

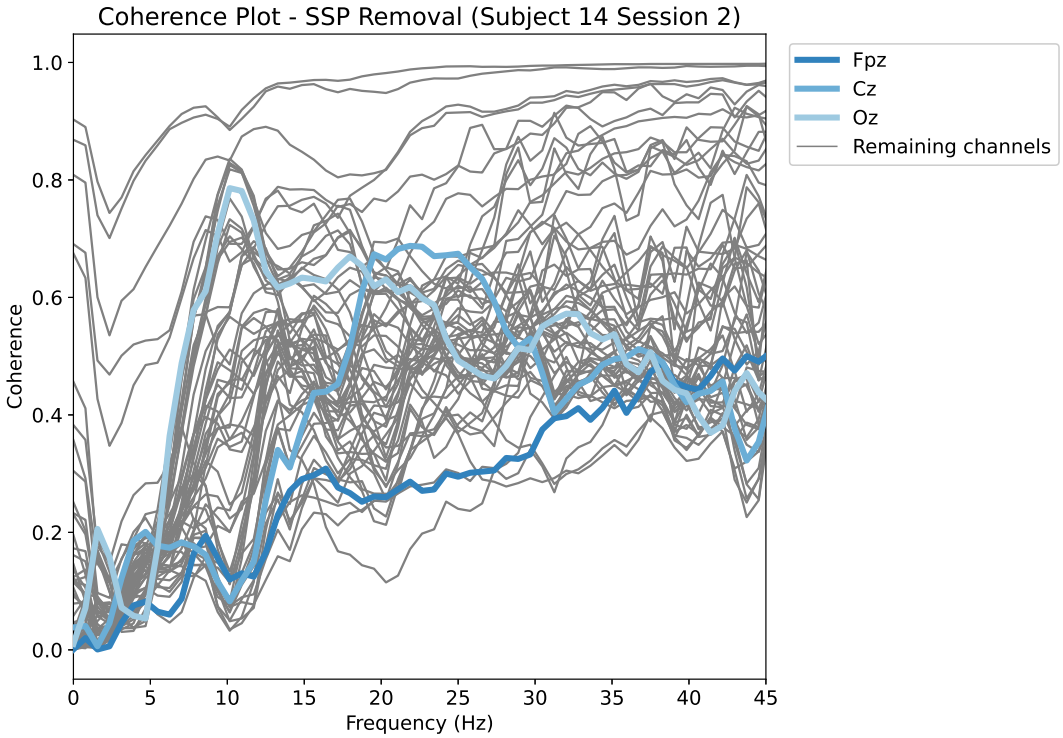

Figure 5.8: The coherence between the channel data from the second session of subject 14, before and after applying SSP. Each line represents the coherence of one channel. Three of the channels are colored as shown in the legend.

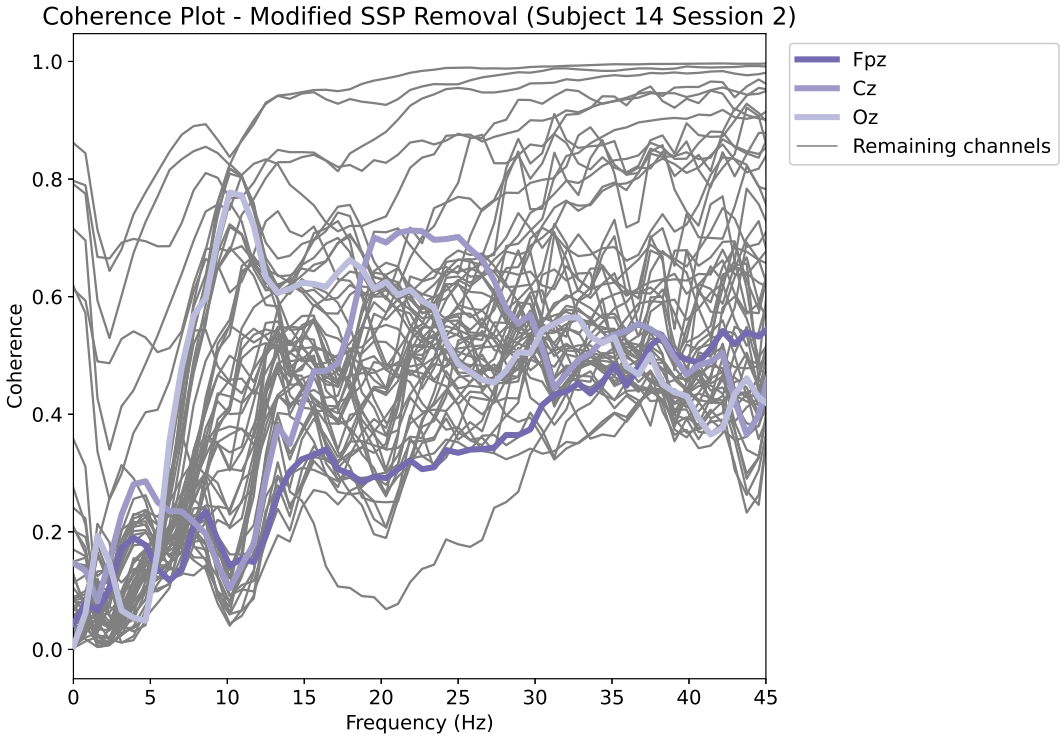

Figure 5.9: The coherence between the channel data from the second session of subject 14, before and after applying the modified version of SSP. Each line represents the coherence of one channel. Three of the channels are colored as shown in the legend.

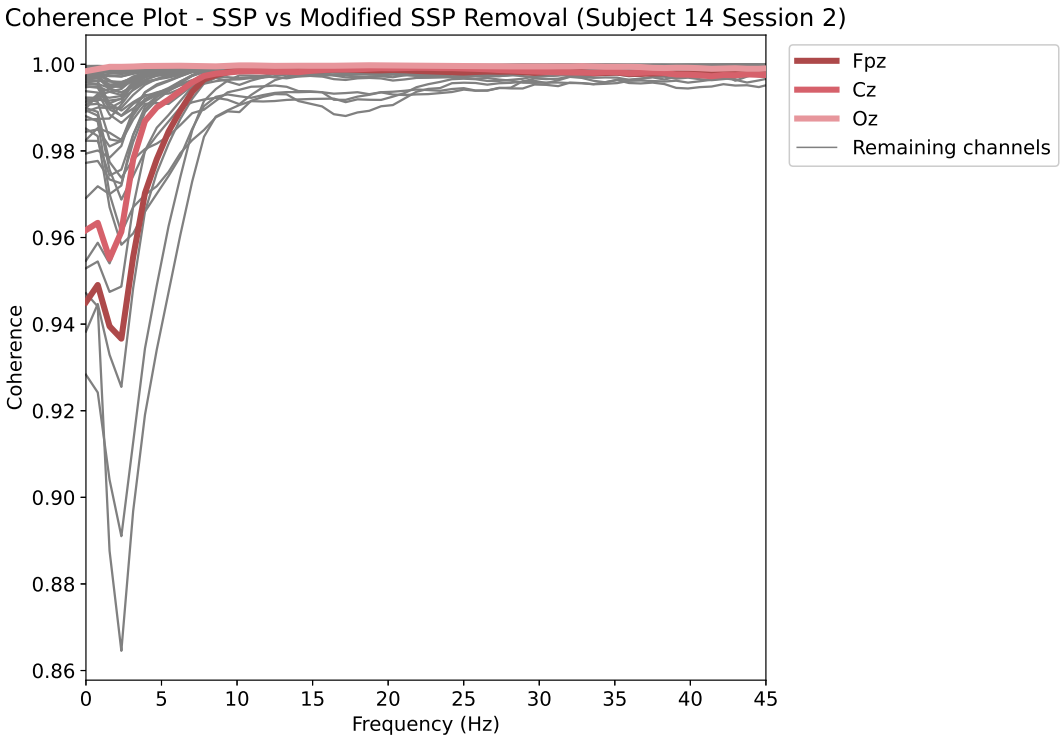

Figure 5.10: The coherence between the channel data from the second session of subject 14, after applying SSP and the modified version of SSP. Each line represents the coherence of one channel. Three of the channels are colored as shown in the legend.

obtained from the two SSP methods supports the validity of the proposed modified SSP method, provided that SSP does indeed preserve the signal integrity. This will be further evaluated using the classification results.

5.2 Classification

The data was put through the preprocessing and the subsequent OA removal techniques as described above. The result was five signals that were then put through classification using *EEGNet* as described in section 4.5. The findings from that classification are presented in this section.

While accurately classifying the appropriate color from the EEG recording is an essential aspect of a BCI, for this particular project it will be adequate to use it as a measure to assess the effectiveness of the various removal techniques. The *EEGNet* model was primarily set up with standard parameters, meaning that the model itself may not be the most optimal choice for this classification task. As a result, the obtained results primarily serve the purpose of comparing the impact of different methods on the classifier, rather than evaluating the classifier's performance. This also pertains to the protocol for the data collection. The effectiveness of the data collection protocol typically plays a crucial role in evaluating classification results. However, due to the potential obscuring effects of ocular artifacts on the collected epochs, the protocol itself cannot be accurately evaluated in this context.

The dataset contains data from 58 channels, however, the primary region responsible for visual pro-

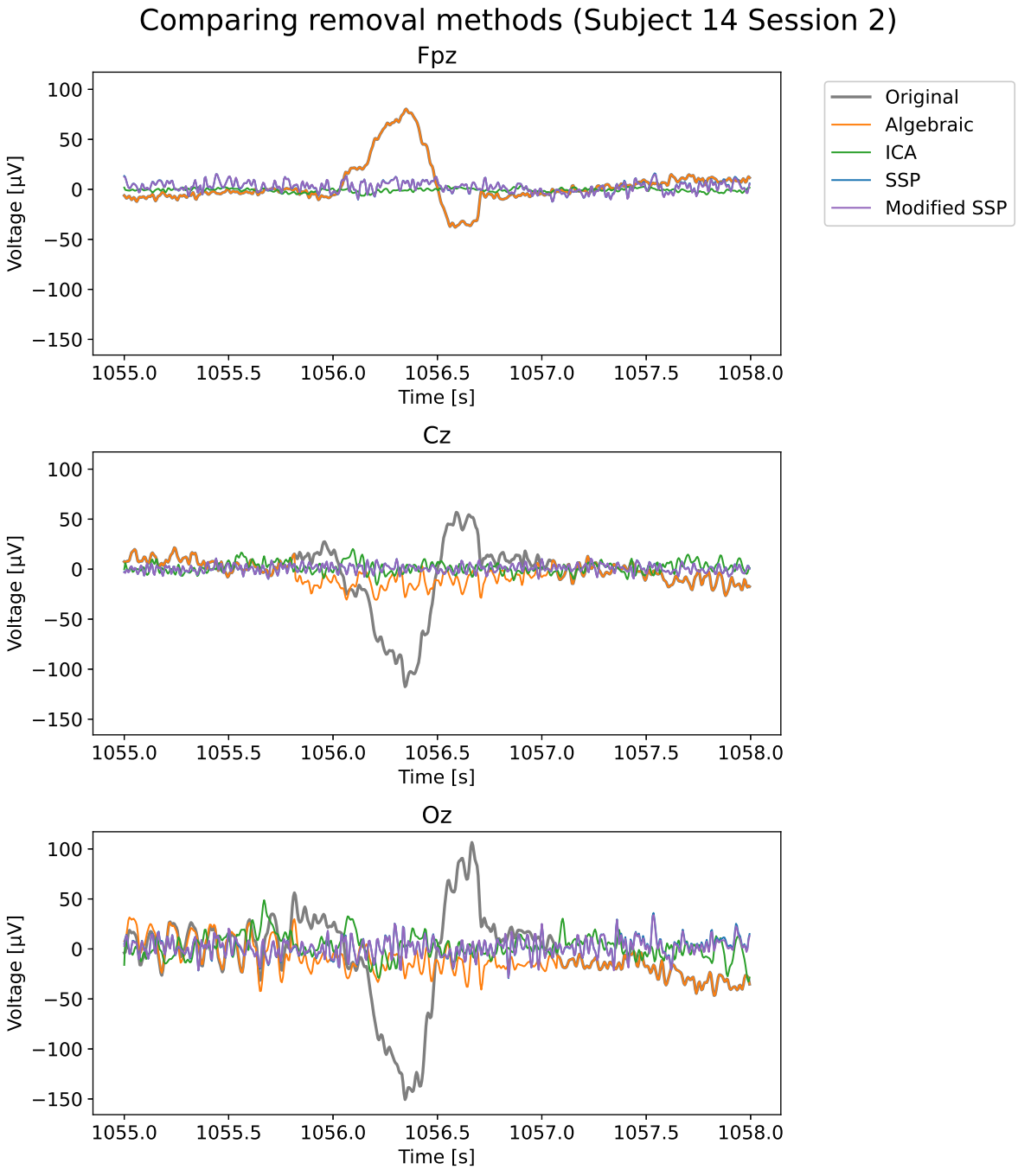

Figure 5.11: An example of a single OA from the second session of subject 14, comparison of the signal after each removal technique for a single artifact for three channels. The two SSP methods resulted in barely distinguishable signals.

cessing in the brain is the occipital lobe. This region is specifically covered by six channels: 'PO3', 'POz', 'PO4', 'O1', 'Oz', and 'O2'. Two models were developed for each subject using data from all 58 channels, and the listed six channels exclusively. These models are referred to as the 58-channel model and the 6-channel model, respectively, and their results are presented in sections 5.2.1 and 5.2.2. Each section presents a figure of the accuracy of the LOOMs created with the data processed in the five different ways: only applying preprocessing, or applying one of the four OA removal methods. These results are presented for each of the subjects. Furthermore, confusion matrices are included, combining the results across all subjects, for each method. Finally, a box plot of the accuracies obtained from the 6- and 58-channel models are presented, for comparing the results obtained for each method.

During the visual inspection of the signal processed using ICA, a minor delay was observed. To address this issue, a uniform delay was applied to all channels, though, there was a slight variation in the delay across individual channels. This was done before the signal was divided into epochs to ensure that the correct data was still contained within the correct epoch and corresponding class. For the rest of the removal methods, the signal was simply split into epochs without any further processing.

5.2.1 6-channel Model

This experiment aimed to investigate the impact of using only the channels in the occipital lobe on classification results. The decision to focus on the occipital lobe was motivated by its known significance in visual processing and its relevance to the task at hand. Reducing the number of electrodes can significantly alleviate the computational complexity of EEG data processing. With a smaller electrode set, the overall dimensionality of the input data decreases, making it computationally more efficient to train and evaluate the classification model. This efficiency is particularly valuable in real-time applications, such as everyday usage of BCIs, where fast processing is crucial. Additionally, from a user's perspective, using fewer electrodes in a BCI setup can enhance comfort and usability. Comparing the effect of using only occipital electrodes with the different OA removal methods is of particular interest. Evaluating the classification performance with reduced electrodes allows for a focused investigation of how different OA removal techniques perform under such conditions.

Applying ICA, SSP, modified SSP and only preprocessing resulted in approximately the same average accuracies of respectively 0.75, 0.69, 0.71, and 0.71, visualized in fig. 5.12. The model for the algebraic method performed the worst with an average accuracy of 0.5, meaning that the model is essentially a random classifier having approximately the same distribution across both true and false predictions. The confusion matrices combining the results of all LOOMs for each of the OA removal methods are presented in fig. 5.13. The four preprocessing pipeline models obtaining the best accuracies had quite balanced matrices, having approximately the same percentage of False Positive (FP) as False Negative (FN). Contrarily, the algebraic removal method, which performed the worst, had a slight overweight of task-state predictions.

The similar accuracies of the four methods suggest the processing pipelines produce data that is of similar quality to the CNN. One of the four methods was solely preprocessing without any OA removal

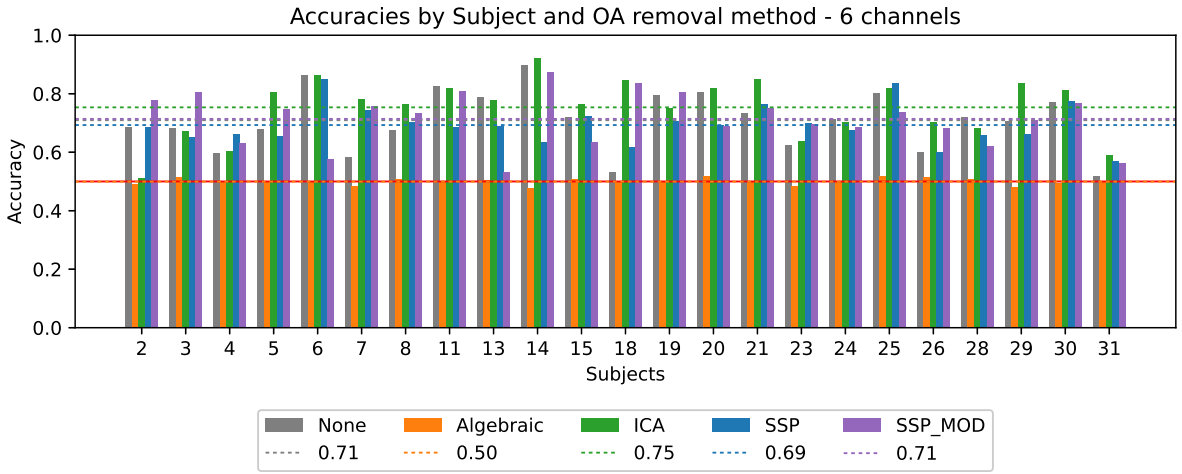

Figure 5.12: Rest vs. task classification accuracies from the LOOMs for each removal technique, using only data from the 6 electrodes in the occipital lobe. The dashed lines are the average accuracy of each method. The average for 'None' and 'SSP_MOD' are coinciding. The random classifier accuracy is marked with a red line, and is coinciding with the average of 'Algebraic'.

technique, and yet achieved similar accuracies to the other methods. It is possible that the processing methods, including OA removal techniques, do not improve the quality of the data significantly for this specific classifier. CNNs are specifically designed to automatically learn and extract meaningful features from the data. Since the performance was approximately the same for the preprocessed data as the data applied OA removal, it indicates that the model may have been able to extract the meaningful features despite the OA spikes. Alternatively, it is plausible that while the methods effectively remove the targeted OA, they may also remove some of the informative signals alongside the noise. This could result in a loss of relevant information required for accurate classification. A third possibility is that while the OA removal appears to be satisfactory, there could still be remnants of the spikes that the CNN is detecting. These potential faults in the process could be leading to similar accuracies compared to the purely preprocessed data.

The results obtained from the classification analysis of the dataset indicated that the highest accuracy, as well as the overall average accuracy, were achieved when employing the ICA for the removal of OAs. This finding aligns with the widely recognized status of ICA as a state-of-the-art technique for OA removal in the field.

As the coherence plot (fig. 5.10) between the data processed with the two SSP techniques indicated, the two methods produced highly similar results. This similarity was also evident in the classification outcomes, as both models yielded very comparable accuracies. Notably, the proposed modified technique exhibited a higher average accuracy compared to the conventional SSP denoising method. Examining the models generated from the dataset processed with SSP, it was observed in fig. 5.13 that they had a slightly lower FP rate but a higher FN rate. Although the difference was not substantial enough to draw definitive conclusions regarding the superiority of one method over the other, it does provide a valuable indication of the efficacy of the SSP approach when utilizing a simulated

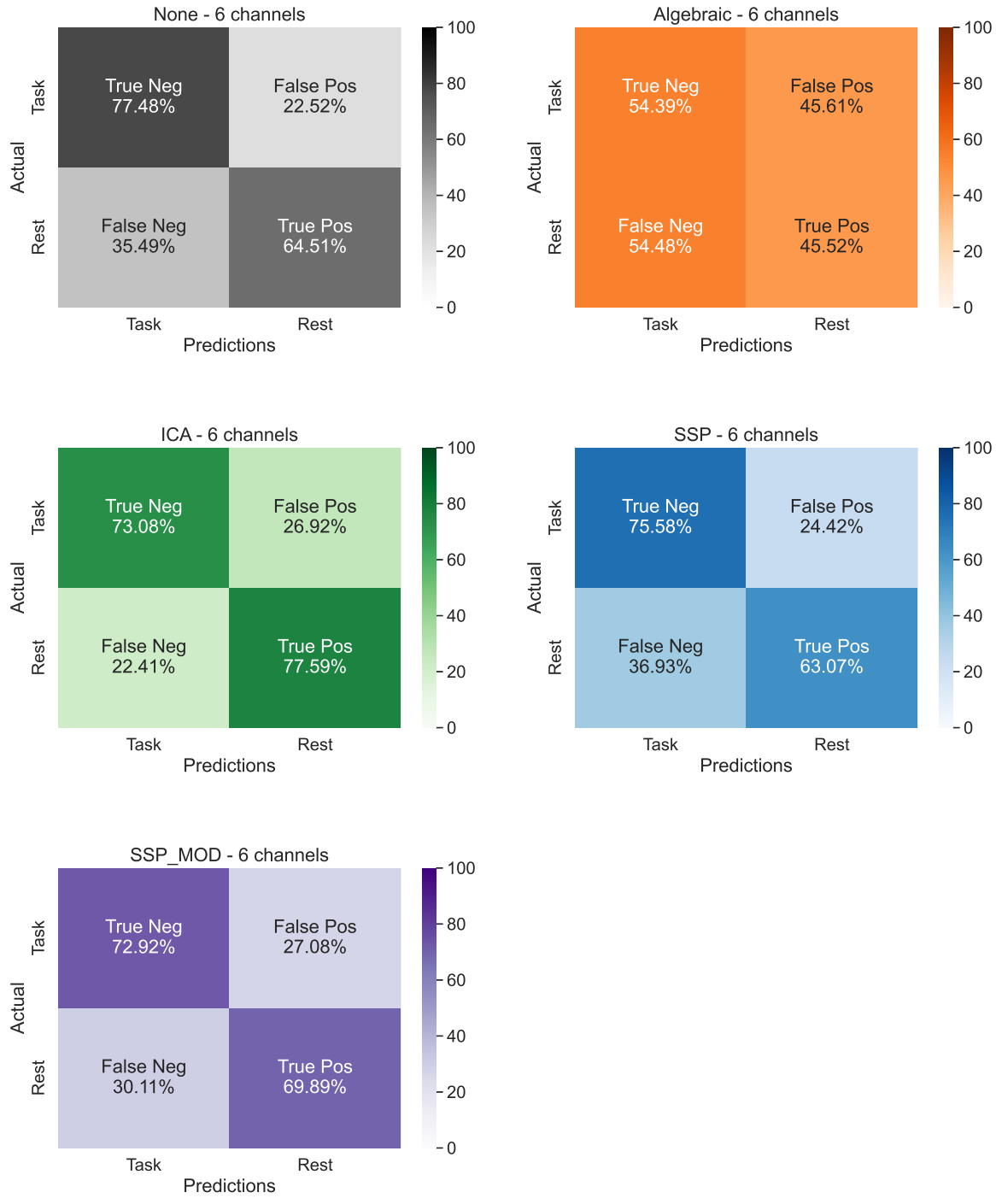

Figure 5.13: Confusion matrices for the rest vs. task classification done using 6 channels for each removal technique.

calibration method for achieving effective overall artifact removal.

The 6-channel models from the signal that was applied the algebraic removal performed the worst out of all when evaluating based on the accuracies. These results could mean that the classifier was not able to differentiate between the task and rest state when the OAs were removed. However, since the three other OA removal methods gave better results, this is not very plausible. One possible interpretation is that the algebraic method, may not adequately preserve the underlying patterns or features in the EEG data that are crucial for accurate classification. This could result in a loss of discriminative information, leading to the lower accuracies observed. Another explanation is that the method may introduce noise to the signal that affects the performance of the CNN. The voltage drop, mentioned in section 5.1.1 and seen in fig. 5.2, is one example of such introduced noise. When the algorithm inputs the recomposed, denoised signal, there is no guarantee that the transition sample values will be close to each other, which can lead to the observed voltage jumps. Moreover, the sudden transition of the denoised signal and the original signal may introduce new nonlinearities. These types of artifacts introduced by the algorithm may contribute to the poor classification results.

Due to the variability in detection accuracy across different channels, as mentioned in section 5.1.1, the resulting channel data will exhibit a varying number of remaining spikes. As a result, there will be an imbalanced spike distribution across the entire dataset. This non-uniform distribution introduces challenges during the classification phase, as the NN model relies on consistent and representative patterns to effectively differentiate between the two classes. Uneven spike counts across channels may skew the learning dynamics and the model's ability to generalize and accurately classify unseen instances may be compromised. Moreover, the imbalanced spike distribution can lead to inadequate feature representation within the CNN model, as the model may fail to recognize the discriminative features.

5.2.2 58-channel Model

This experiment aimed to assess the impact of utilizing all 58 channels in the classification results. Although the focus on the occipital lobe is motivated by its known significance in visual processing and its relevance to the task, it is also important to investigate the performance when using a larger number of electrodes. Evaluating the performance of the various OA removal techniques using the complete electrode setup allows for a comprehensive assessment of their efficacy under more complex electrode configurations.

Although more information is available, the performance generally decreased for the 58-channel models compared to the 6-channel. As seen in fig. 5.14, the average accuracy of the models created with the five processing pipelines were 0.66, 0.51, 0.61, 0.69, and 0.66 for data applied only preprocessing, algebraic removal, ICA, SSP and the modified SSP, respectively. The results show that one of the models generated from data with no OA removal gave the highest accuracy of all models. This finding challenges the assumption that utilizing artifact removal techniques leads to improved classification accuracy. The confusion matrices generated for these models are presented in fig. 5.15. There is generally less balance in the FP and FN predictions using the whole dataset.

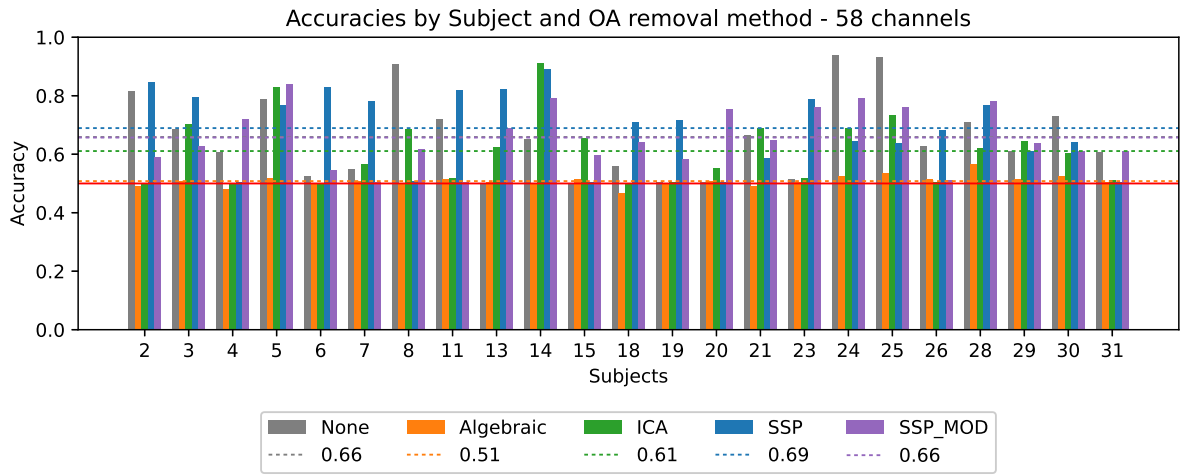

Figure 5.14: Rest vs. task classification accuracies from the LOOMs for each removal technique, using all 58 channels. The dashed lines are the average accuracy of each method. The average for 'None' and 'SSP_MOD' are coinciding. The random classifier accuracy is marked with a red line, and is coinciding with the average of 'Algebraic'.

Contrarily to the 6-channel model, data that was applied ICA removal had one of the lowest accuracies, with only the algebraic removal that gave random classifier results, performing worse. The majority of errors in these cases were false positive rest-state classifications.

By using the whole set of channels, conventional SSP gave on average better results than the modified. This suggests that the standard SSP approach, without modifications, was more effective in mitigating artifacts and improving classification accuracy when more data was used.

Similar to the findings in the 6-channel model, the application of algebraic removal to the 58-channel data did not improve classification accuracy. The average accuracy was 0.51, with a slight overweight of rest classifications, as seen in fig. 5.15 in contrast to the 6-channel model.

5.2.3 Comparison of Classification Results

Figure 5.16 compares the accuracies obtained when training the CNN on data with the different OA removal techniques. There is a larger interquartile range for the models using all channels, meaning there is variability in the results obtained from those models.

Generally, there is a trend of worse performance when using all the channels. When the input contains irrelevant information, such as noise or artifacts, it can hinder the network's ability to extract relevant features and make accurate predictions. The presence of additional channels in the 58-channel setup could have introduced more noise or irrelevant information into the input data, making it more challenging for CNN to discern important patterns. As a result, the overall performance of the models created with the 58-channel setup suffered compared to the 6-channel models.

ICA produced the greatest difference in model results when using the total dataset. The results visu-

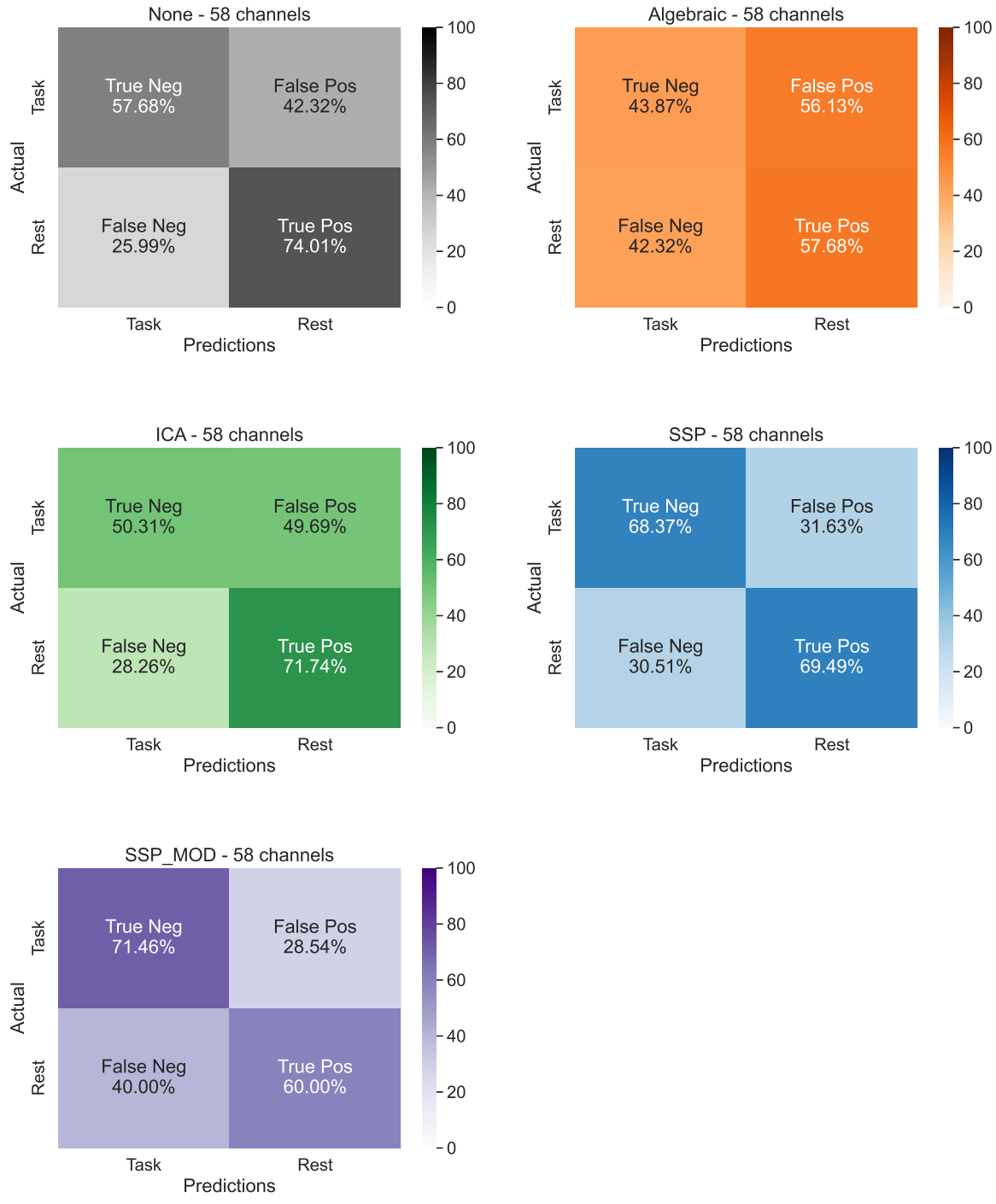

Figure 5.15: Confusion matrices for the rest vs. task classification done using 58 channels for each removal technique.

alized in fig. 5.16 show that only 25% of the models had a resulting accuracy of over 70%, while for the models using the 6 occipital lobe electrodes, approximately 75% of the models had accuracies above 70%. Because of the better performance using data from the relevant area of the brain, this indicates that the fault stems from the use of too many irrelevant channels and not from a poor artifact removal method.

The models generated from the dataset employing the modified SSP artifact removal exhibited the smallest disparity between the 58- and 6-channel model results, in contrast to the other OA removal models. Notably, the signal subspace estimation was performed using the same number of channels as the model, suggesting that the estimation remains reliable even when utilizing a limited number of channels. This finding underscores the robustness and efficacy of the modified SSP artifact removal method in achieving consistent performance across different channel configurations.

Overall, there is a general trend of a lower variation of the model accuracies in the 6-channel models compared to the 58-channel models suggests an enhanced generalizability when utilizing fewer channels. The models trained on fewer channels are better at capturing the essential features and patterns that are consistent across multiple channels, leading to improved performance across different datasets and scenarios. Thus, the utilization of a smaller set of channels can contribute to increased robustness and generalizability of the models in the context of OA detection and classification.

For the algebraic method, the accuracy obtained from the 58-channel data was slightly increased from that of the 6-channel model. As discussed in section 5.1.1, the detection of the OAs in the occipital lobe was too sensitive, and overestimated the number of spikes in the signal. Consequently, a larger portion of the data is exchanged with the reconstructed, denoised data. In this process, the data can lose some information crucial to the feature extraction in the CNN, resulting in poor classification results. As also discussed, the detection was more accurate in the central channel and underestimated the number of OAs in the frontal channel. When creating models from all the channel data, a larger portion of the original signal is left. However, this data may be less relevant to the visual stimuli. This may have contributed to the slight increase in performance and would support the theory of the algebraic removal method removing too much information from the signal.

A notable observation shared by the models developed from both the 6-channel and 58-channel data is the inter-subject variation in individual performance. Emphasizing the subject-wise performances is crucial, as the application of potential BCI systems is inherently personalized. In figs. 5.12 and 5.14, it is evident that certain subjects consistently achieved better results across different processing methods, such as subject 14, who exhibited the highest accuracy for multiple models. Conversely, subject 31 consistently performed below the average for models derived from all methods. Likewise, several other subjects displayed a higher proportion of lower model accuracy, exemplified by subject 31. These findings indicate the presence of individual subject characteristics that influence the performance of the models. One possible explanation for the observed differences could be the presence of fewer artifacts or better recording quality for certain subjects. Understanding and accounting for these subject-specific factors will be essential for the successful implementation of a personalized BCI system.

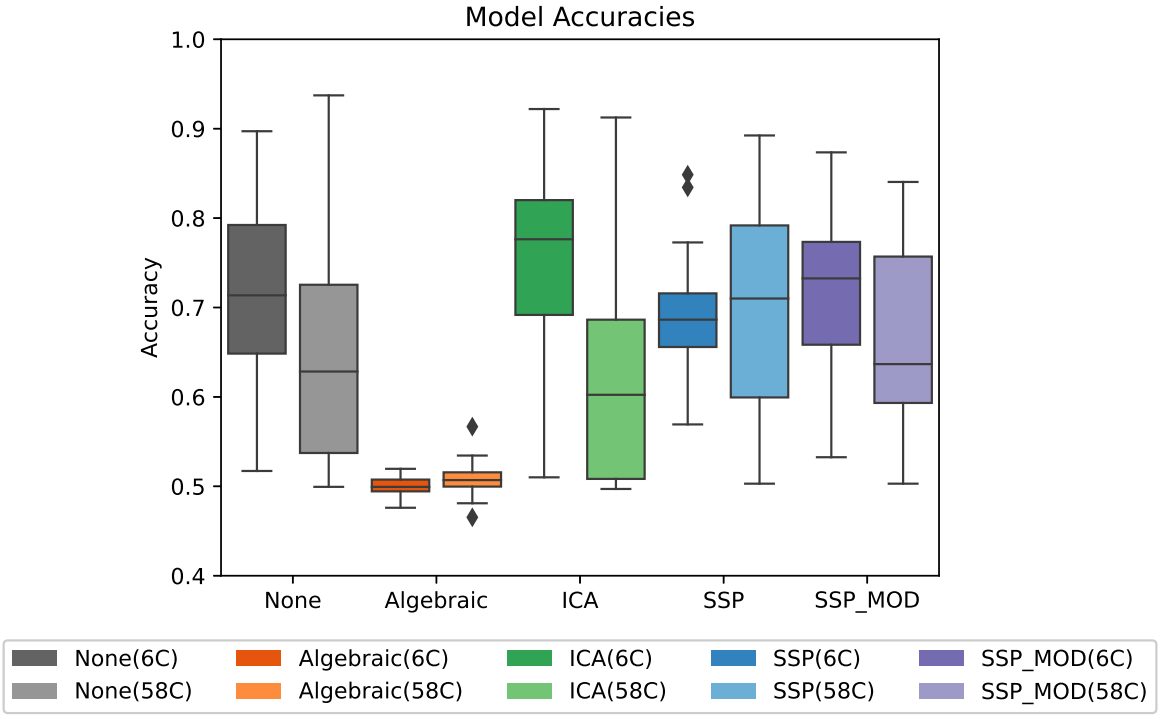

Figure 5.16: Comparison of the accuracies from the 6- and 58-channel models for each OA removal technique. The darkest colors illustrate the accuracies obtained from classification using 6 channels, while the lighter colors illustrate the accuracies from classification using 58 channels.

Chapter 6

Conclusion, Discussion and Further Work

6.1 Discussion

The aim of this work was to investigate methods for removing OA from recorded EEG signals and evaluate the effectiveness and feasibility of usage in a future BCI. Four different techniques were tested, ICA, an algebraic approach, and two versions of SSP. Classification using CNN was then used as an additional evaluation framework for artifact removal.

The objective is motivated by the wish to ease the life of individuals with LIS. Effective communication plays a crucial role in an individual's autonomy and overall well-being. However, the existing communication aids used in LIS often come with the disadvantage of being time-consuming, making it challenging to participate in conversations and significantly prolonging the duration required to communicate a single sentence. In addition to this, the method also lacks privacy for the user, as mentioned in chapters 1 and 3. By leveraging BCI technology, a more efficient and accurate communication approach can be established, potentially alleviating the negative impact of the current communication methods on the individual's quality of life.

When investigating the methods for developing a BCI based communication, processing pipelines for the EEG signals are an important part. In this work, specifically, the noise-reducing methods of OA removal were implemented and evaluated for use in BCIs. The current state-of-the-art method for removal of the spikes introduced to the signal due to blinks is ICA, however, because of the computational heaviness, it is not suited for real-time applications, such as BCIs. SSP is a similar method, also too computationally heavy for BCIs because the method requires an extraction of OAs to calculate the projection that is applied to the whole signal.

Two methods for real-time usage were implemented and tested. Firstly, a method proposed by [47], of a hybrid OA detection and removal algorithm. Secondly, a proposed method, that uses the projection

similarly as in SSP, but by using a defined interval to find the artifacts.

6.1.1 Dataset

A high-quality dataset is crucial for data analysis when it comes to ensuring the accuracy and reliability of the findings. The dataset used in this project was gathered in a controlled and stable environment. It has been previously employed in classification tasks and demonstrated satisfactory performance [4], indicating its suitability. In this study, epochs that contained artifacts such as blinks or muscle movements were systematically excluded. As this project aims to investigate various methods for OA removal, the dataset selected is deemed appropriate. Moreover, since participants were instructed to blink during pauses rather than RGB colors, the epochs containing OA are overrepresented during the pauses. This makes for uncertainties, as the two classes might have seen different processing.

6.1.2 Ocular Artifact Removal

The experiments performed for this project were designed to test out the effects of the different artifact removal techniques and the subsequent classification using the processed data. Using visual inspection of the signal as well as an inspection of the coherence between the processed signals and the original recording, it was found that most of the methods were detecting and removing the spikes caused by the OA to a satisfactory degree. The second objective was to find the best method to differentiate between a task state and a resting state as a way to compare the acoa removal.

The results obtained from the 6- and 58-channel models are summarized in table 6.1. The experiments showed that models created with 6 channels gave on average better results, while the 58-channel models had the total highest accuracy. The best performing method was ICA for the 6-channel models and no acoa removal for the 58-channel models. The algebraic method performed poorer, with variation in OA detection across the different channels causing the resulting signal to either remove too few artifacts or applying the removal algorithm where it was not needed. This tendency was also seen in the classification, as the rest of the models achieved average accuracies of 69-75% while the one based on the algebraic method behaved close to a random classifier at 50%.

Examining the individual accuracies across both the 6-channel and 58-channel models in table 6.1, it is evident that the "None" method yielded the highest accuracy (0.94 for 58 channels) and the second-highest accuracy for 6 channels. This suggests that not applying any specific artifact removal technique may result in relatively better performance in terms of classification accuracy. Though, because the dataset contains OAs in the resting states, the classifier may discriminate between blink vs. no blink rather than color vs. no color.

For each of the methods to be working as efficiently as possible, there is a need to tune them to fit the signal. For the ICA the algorithm is provided by *MNE* and only requires some visual inspection, which can be aided by the other working analysis tools of *MNE*. Similarly, for the SSP, the built-in features of *MNE* take care of calculating the subspace provided the signal and the desired number of vectors. In this work, it has been found the output can be affected by calculating the subspace

Method	6 channels		58 channels		Method suitable for real-time
	Average	Best (subject)	Average	Best (subject)	
None	0.71	0.90 (14)	0.66	0.94 (24)	Yes
Algebraic	0.50	0.52 (20)	0.51	0.57 (28)	Yes
ICA	0.75	0.92 (14)	0.61	0.91 (14)	No
SSP	0.69	0.85 (6)	0.69	0.89 (14)	No
SSP_MOD	0.71	0.87 (14)	0.66	0.84 (5)	Yes

Table 6.1: Summary of the obtained results from the rest vs. task classification after each method for artifact removal. The table presents the average accuracies of the LOOMs created using each method of 6- and 58-channel data. The table also presents the maximum accuracy obtained for each method, and the subject yielding the result.

on a different segment than the vectors are applied to. Lastly, the logic of the algebraic method has been implemented by hand and is therefore the most likely to be prone to error handling due to implementation and non-established tuning processes.

The variation in detection across channels has likely contributed to the poor performance of the algebraic method. The threshold used for detection was tuned by visual inspection across different subjects in an effort to find a value that would perform in a generally satisfactory manner for all the subjects. However, upon reviewing the obtained results, it is evident that additional calibration of the algorithm is required, both on an individual subject basis and for each individual channel.

A potential approach for calibration could be implemented similarly to the proposed method for the modified SSP. This could involve allocating a brief initial period during a user session, which would serve as the basis for calculating the detection threshold. In order to ensure a more consistent detection and removal process across all channels, a decision function for detection could be implemented. In this function, the cumulative detection results across channels would establish a global OA-zone. This would compensate for under-detection in the frontal channels by incorporating detection from other channels, while over-detection in the occipital channels would be counterbalanced by the absence of detection in the remaining electrodes. Alternatively, it would be possible to implement separate thresholds for each channel, allowing the detection to be independent of the performance of other thresholds.

When suggesting a calibration process for the detection threshold, it is imperative that the equation used is also considered as a potential contributor to the underperformance. The equation for the threshold, obtained from [47], is presented in equation eq. (4.1). The observed variations in results across channels align well with the fact that the equation is inversely proportional to the SD, as discussed in section section 5.1.1. It is important to further investigate the relationship between the SD of the signal and the spike amplitudes caused by OAs. Adjustments to this equation may be necessary to establish a threshold that can be applied consistently across channels and subjects. This could involve exploring alternatives such as an inversely proportional relationship or entirely differ-

ent threshold formulations.

The similarity in performance between the two versions of SSP are indicative of the feasibility of developing a calibration process for calculating the noise subspace. These results highlight the potential of the proposed modified SSP method as a viable approach for OA removal. Moreover, the method's ability to maintain high accuracy while offering real-time feasibility positions it as a valuable candidate for future exploration and development in the field of BCI systems. The calibration segment was extracted from the pause in the data protocol, but it was noted that this section contained artifacts other than eye blinks and small movements resulting from fixating on the screen, likely due to subjects' movement and speaking. Since both versions of SSP exhibited similar performance using different segments, it would be beneficial to further investigate the influence of what kind of segment is used for the calibration. Exploring the effects of using different segments, such as one from the middle of the protocol that reflects activity levels during actual use, as well as that of the actual patient group, could provide valuable insights. This analysis of various data segments would contribute to understanding the limitations and requirements of this calibration method, ensuring its robustness, which is crucial for its application in a BCI setting.

The over-representation of the OAs in the epochs representing the rest state creates a potential risk of the classifier learning a spurious association between the presence of OAs and the classification task. This is especially relevant for ML models that rely solely on the preprocessed signal, in which the OAs remain. Comparing the performance of these models with other methods reveals minimal differences. There are several possible explanations for this finding. Firstly, the CNN might be capable of sufficiently identifying the underlying features related to color perception in the EEG data, enabling it to overlook the artifacts on its own. Alternatively, the CNN may still be detecting artifacts even after removal, either due to incomplete artifact removal or the introduction of new noise during the removal algorithms. To investigate this, it would be valuable to examine how epochs containing artifacts are distributed within the confusion matrix, providing insights into the impact of artifact removal on classification performance. Additionally, employing alternative classifiers such as RF and SVM, which are not based on deep learning, may yield more pronounced differences in classification results. These classifiers also offer enhanced model transparency and the ability to determine feature relevance, which could provide a further understanding of the features employed in the classification process.

During the implementation of the classification, the choice was made to not include epoch rejection as this was likely to affect the OAs, especially for the algebraic method, and the signal simply undergoing preprocessing. This means that there may very well have been left other types of artifacts in the signal, that might have influenced the classification. However, it is reasonable to assume that the distribution of these artifacts is approximately equal between the two classes. Therefore, the presence of these epochs should have minimal impact on the evaluation of the OA removal methods.

It is important to note that the performance was heavily influenced by subject-specific variations. Subject 14 often achieved the best accuracy using the varying methods, yielding the best accuracies for five out of the ten maximum accuracies presented in table 6.1. Though this session was chosen

to highlight the typical response of the removal process, its high performance for the classification was not anticipated. It may very well be due to individual differences in the quality of the recordings. These results underscore the importance of considering subject-specific variations, as some subjects consistently outperformed others across different processing methods. Such subject-specific performance variations emphasize the importance of personalized approaches in the development of BCI systems.

Limitations have been encountered in the evaluation of the results obtained from this project. Although adjustments have been made to the signal within the desired range based on coherence plots, it remains unclear what noise has been introduced to the signal. Initial visual inspections suggest a satisfactory signal appearance, but a deeper analysis using additional tools is necessary to explore the underlying structures and features of the signal. Since the classification results may merely distinguish epochs that contain OAs from those without, further evaluation of the methods is needed before protocols and the next steps toward BCIs are discussed.

6.1.3 Towards a BCI

The methodologies assessed in this research project rely on the utilization of EEG to capture signals from patients. Although the selection of this method is motivated by its cost-effectiveness and user-friendly nature, requiring minimal cognitive exertion, it is imperative to examine the patients' perception and acceptance of this approach. The study [65] presented in section 3.1 reported that the preferred method for the use of BCIs was speech, followed by attempted movement. This raises the question of the relevance of pursuing approaches that may not be in line with the patients' wishes. However, as discussed in section 3.1 there has been reported promising result regarding EEG-based BCIs.

The utilization of visual stimuli as the cognitive strategy for operating a BCI necessitates users' control over certain eye movements and blinking. This requirement may lead to a lack of inclusivity for patients with CLIS. Considering that patients with incomplete LIS may retain some degree of bodily movement, it is improbable that they would find this approach useful, as attempted movements are typically more favored as a cognitive strategy. However, a recent study [93] examined the potential of employing imagined colors as a means of controlling a BCI and reported promising outcomes, indicating the feasibility of this method. Implementing this approach could enhance inclusivity for patients with CLIS, offering them an alternative means of interaction.

The requirements for the protocol accompanying the BCI implementation also warrant consideration. In order to offer advantages over existing keyboards that utilize eye tracking, the method should incorporate a predefined set of commands that enable swift communication. This feature is essential for facilitating rapid and efficient interaction, ensuring that the proposed method surpasses the functionality of current eye-tracking keyboards.

6.2 Conclusion

This work aimed to investigate methods for removing OAs from EEG signals and evaluate their effectiveness for potential use in a future BCI communication system for individuals with LIS. The motivation behind this research stems from the need to improve communication methods for individuals with LIS, who face significant challenges due to their limited motor control and speech capabilities. By harnessing BCI technology and EEG signals, a more efficient and accurate communication approach can be developed, potentially enhancing the quality of life for individuals with LIS. Three techniques, including ICA, SSP, and an algebraic method, were tested and compared in terms of OA removal and their impact on classification performance.

The experiments conducted in this study focused on the removal of OAs from EEG signals using different techniques. Visual inspection and coherence analysis demonstrated that most of the methods effectively detected and removed the artifacts caused by eye blinks. However, the algebraic method showed poorer performance, with variations in OA detection across different channels. The classification results also revealed that the other models achieved average accuracies of 69-75%, while the algebraic-based model behaved close to a random classifier at 50%. Among the real-time suitable techniques for removal, the modified SSP method yielded the highest average accuracy of 71%. Nevertheless, due to variations in individual performance, the best result achieved by an individual subject was 94% without using OA removal. The presence of OAs in the rest state epochs posed a potential risk of false associations between artifacts and the classification task. However, the performance of ML models, particularly CNNs, did not show significant differences when comparing models using preprocessed signals with and without OAs. Further analysis, such as examining the distribution of epochs containing artifacts within the confusion matrix, and exploring alternative classifiers, could provide a deeper understanding of the impact of artifact removal on classification performance.

OA removal methods a calibration processes and adjustments to the detection thresholds were proposed. The implementation of individual subject-based and channel-specific calibration could improve the consistency and performance of the removal algorithms. Moreover, further investigation into the relationship between the SD of the signal and OA spike amplitudes could lead to refinements in the threshold equation. The evaluation of two versions of SSP indicated the feasibility of developing a calibration process for calculating the noise subspace. Exploring different data segments for calibration, including segments from the middle of the protocol and those representing actual patient data, would provide valuable insights into the limitations and requirements of this calibration method.

In conclusion, this work has contributed to the exploration of artifact removal methods for potential use in a BCI-based communication system for individuals with LIS. While improvements and optimizations are still needed, the findings support the feasibility of developing efficient OA removal process for BCIs, that could be used in accurate communication platforms. The results have also highlighted the importance of investigating different types of classifiers and their need for effectively removing OAs.

6.3 Future Work

The end goal of this thesis is to evaluate methods for signal processing with the end goal of creating an EEG-based BCI. Keeping this in mind when moving forward is important, to ensure the patients' needs are being assessed, and that the approaches are well-suited for this type of real-time application.

Further refinement of these methods for OA removal is crucial if they are to be relevant for this task. Both the algebraic method and the modified version of SSP are in need of working calibration protocols that will ensure they are tailored to each individual as well as the patient group. For this, the SSP should be tested on calibration segments that are more similar to that of the patient group, if not actual patient data. Should there be developed a calibration system for the algebraic method rendering it more robust across channels, there could be a cause to investigate this method further. Although, for now, there appears to be more promise in pursuing the SSP as a method for artifact removal.

Though not the focus of this thesis, having a BCI as the end goal means the classification also needs to be improved further. The promising results achieved with *EEGNet*, indicate that the NN is quite capable of classifying the two tasks. Given that EEGNet performed quite well without the artifact removal, utilizing a classifier that is not based on NN, but rather more dependent on the signature of the features being preserved through the process could prove useful. This could be classifiers such as RF or SVM that may compute feature importance analysis and thereby provide interpretable models that could identify the most important factors in the classification process. This could help shed more light on the differences between the original and the processed signal.

An option that should be considered for the data is to create a dataset with synthetic OAs. This would allow for further analysis of the impact of both the OAs and the removal processes on the signal and the subsequent classification. It would also allow for the epochs affected by OAs more evenly distributed between the two tasks, ensuring that there is no bias toward one of the classes. This would make sure that the original signal could serve as a more accurate benchmark for the removal than that of the ICA.

With the BCI in mind, further testing of the approach should go toward ensuring online functionality that is tailored towards the patient group. This means evaluating the computational demands and time performance of the methods, in order to optimize the real-time performance of the system. This also includes shortening the length of the epochs, while keeping up the classification performance. As reported by persons with LIS, the time it takes to efficiently communicate should be one of the priorities in the development of assistive technologies. Maintaining focus on this entails discussing designs with persons with LIS as well as their caregivers and ensuring that no requirements are lost in the process.

References

[1] Sandra Garder Løkken. Ocular artifact detection and removal for eeg-based applications using algebraic detection and dwt thresholding. Project thesis, Norwegian University of Science and Technology, Trondheim, December 2022.

[2] Mari Hestetun Dokken. Detection and removal of ocular artifacts in eeg-based applications using algebraic detection and dwt thresholding. Project thesis, Norwegian University of Science and Technology, Trondheim, January 2023.

[3] Vernon J Lawhern, Amelia J Solon, Nicholas R Waytowich, Stephen M Gordon, Chou P Hung, and Brent J Lance. Eegnet: a compact convolutional neural network for eeg-based brain–computer interfaces. *Journal of neural engineering*, 15(5):056013, 2018.

[4] Sara L Ludvigsen, Emma H Buøen, Andres Soler, and Marta Molinas. Searching for unique neural descriptors of primary colours in eeg signals: a classification study. In *Brain Informatics: 14th International Conference, BI 2021, Virtual Event, September 17–19, 2021, Proceedings 14*, pages 277–286. Springer, 2021.

[5] Tobias Treider Moe. Towards a communication system for patients with locked-in syndrome based on eeg and visual perception. Master thesis, Norwegian University of Science and Technology, Trondheim, June 2022.

[6] Steven Laureys, Frédéric Pellas, Philippe Van Eeckhout, Sofiane Ghorbel, Caroline Schnakers, Fabien Perrin, Jacques Berre, Marie-Elisabeth Faymonville, Karl-Heinz Pantke, Francois Damas, et al. The locked-in syndrome: what is it like to be conscious but paralyzed and voiceless? *Progress in brain research*, 150:495–611, 2005.

[7] Liesbet Snoeys, Gertie Vanhoof, and Eric Manders. Living with locked-in syndrome: an explorative study on health care situation, communication and quality of life. *Disability and rehabilitation*, 35(9):713–718, 2013.

[8] Veronica Johansson, Surjo R Soekadar, and Jens Clausen. Locked out: Ignorance and responsibility in brain–computer interface communication in locked-in syndrome. *Cambridge Quarterly of Healthcare Ethics*, 26(4):555–576, 2017.

[9] NRK. Mathias (21) er norges yngste med locked-in-syndrom. `https://www.nrk.no/osloogviken/xl/mathias-_21_-er-norges-yngste-med-locked-in-syndrom-1.15932211`, 2021.

[10] Fabien Lotte, Laurent Bougrain, Andrzej Cichocki, Maureen Clerc, Marco Congedo, Alain Rakotomamonjy, and Florian Yger. A review of classification algorithms for eeg-based brain–computer interfaces: a 10 year update. *Journal of neural engineering*, 15(3):031005, 2018.

[11] Tobias Treider Moe. Designing an eeg based communication system for patients with locked-in syndrome. Project thesis, Norwegian University of Science and Technology, Trondheim, June 2022.

[12] Xiao Jiang, Gui-Bin Bian, and Zean Tian. Removal of artifacts from eeg signals: a review. *Sensors*, 19(5):987, 2019.

[13] Eimear Smith and Mark Delargy. Locked-in syndrome. *Bmj*, 330(7488):406–409, 2005.

[14] Taras Halan, Juan Fernando Ortiz, Dinesh Reddy, Abbas Altamimi, Abimbola O. Ajibowo, and Stephanie P. Fabara. Locked-in syndrome: A systematic review of long-term management and prognosis, Jul 2021.

[15] Sunnaas Sykehus. Locked-in syndrom. `https://www.sunnaas.no/behandlinger/locked-in-syndrom`.

[16] Kunal Khanna, Ajit Verma, and Bella Richard. The locked-in syndrome: Can it be unlocked? *Journal of Clinical Gerontology and Geriatrics*, 2(4):96–99, 2011.

[17] Elaine N. Marieb and Suzanne M. Keller. *Essentials of Human Anatomy & Physiology*, chapter 7: The Nervous system, pages 246–189. Pearson, 13th edition, January 2021.

[18] Blausen Medical. Medical gallery of blausen medical 2014. *WikiJournal of Medicine*, 1(2):1–79, 2014.

[19] Eric R Kandel, James H Schwartz, Thomas M Jessell, Steven A Siegelbaum, A James Hudspeth, and Sebastian Mack. Low-level visual processing: The retina. In *Principles of Neural Science, Fifth Edition*. McGraw Hill, 2012. Accessed May 10, 2023.

[20] John D Mollon. Color vision. *Annual review of psychology*, 33(1):41–85, 1982.

[21] Karl R Gegenfurtner and Daniel C Kiper. Color vision. *Annual review of neuroscience*, 26(1):181–206, 2003.

[22] Inês Bramão, Luís Faísca, Christian Forkstam, Alexandra Reis, and Karl Magnus Petersson. Cortical brain regions associated with color processing: An fmri study. *The open neuroimaging journal*, 4:164, 2010.

[23] Wikipedia contributors. Visual system — Wikipedia, the free encyclopedia. `https://en.wikipedia.org/w/index.php?title=Visual_system&oldid=1148714425`, 2023. [Online; accessed 26-April-2023].

[24] Introduction to psychology - how we see. `https://courses.lumenlearning.com/waymaker-psychology/chapter/vision/`, (n.d.). Last accessed 04-26-2023.

[25] Mark Bear, Barry Connors, and Michael A Paradiso. *Neuroscience: exploring the brain, enhanced edition: exploring the brain.* Jones & Bartlett Learning, 2020.

[26] Li Hu and Zhiguo Zhang. *EEG signal processing and feature extraction.* Springer, 2019.

[27] Timo Kirschstein and Rüdiger Köhling. What is the source of the eeg? *Clinical EEG and neuroscience*, 40(3):146–149, 2009.

[28] Kannathal Natarajan, Rajendra Acharya U, Fadhilah Alias, Thelma Tiboleng, and Sadasivan K Puthusserypady. Nonlinear analysis of eeg signals at different mental states. *Biomedical engineering online*, 3:1–11, 2004.

[29] Ernst Niedermeyer and FH Lopes da Silva. *Electroencephalography: basic principles, clinical applications, and related fields.* Lippincott Williams & Wilkins, 2005.

[30] Lauren C. Frey St Louis Erik K. and Jeffrey W. Britton. *An Introductory Text and Atlas of Normal and Abnormal Findings in Adults, Children, and Infants.* American Epilepsy Society, Chicago, 2016. Appendix 2.

[31] Steven J Luck. *An introduction to the event-related potential technique.* MIT press, 2014.

[32] Andrea Biasiucci, Benedetta Franceschiello, and Micah M Murray. Electroencephalography. *Current Biology*, 29(3):R80–R85, 2019.

[33] Claudio Babiloni, Robert J Barry, Erol Başar, Katarzyna J Blinowska, Andrzej Cichocki, Wilhelmus HIM Drinkenburg, Wolfgang Klimesch, Robert T Knight, Fernando Lopes da Silva, Paul Nunez, et al. International federation of clinical neurophysiology (ifcn)–eeg research workgroup: Recommendations on frequency and topographic analysis of resting state eeg rhythms. part 1: Applications in clinical research studies. *Clinical Neurophysiology*, 131(1):285–307, 2020.

[34] Abdul Qayoom Hamal and Abdul Wahab bin Abdul Rehman. Artifact processing of epileptic eeg signals: An overview of different types of artifacts. In *2013 International Conference on Advanced Computer Science Applications and Technologies*, pages 358–361, 2013.

[35] Rakesh Ranjan, Bikash Chandra Sahana, and Ashish Kumar Bhandari. Ocular artifact elimination from electroencephalography signals: A systematic review. *Biocybernetics and Biomedical Engineering*, 41(3):960–996, 2021.

[36] Servier Medical Art. Eye. `https://smart.servier.com/smart_image/eye/`, (n.d.).

[37] Otavio G. Lins, Terence W. Picton, Patrick Berg, and Michael Scherg. Ocular artifacts in eeg and event-related potentials i: Scalp topography. *Brain Topography*, 6:51–63, 1993.

[38] Danny Oude Bos. Automated artifact detection in brainstream, 2012.

[39] W. Barry and G.M. Jones. Influence of eye lid movement upon electro-oculographic recording of vertical eye movements. *Aerosp Med*, 36:855–858, 1965.

[40] Masaki Iwasaki, Christoph Kellinghaus, Andreas V. Alexopoulos, Richard C. Burgess, Arun N. Kumar, Yanning H. Han, Hans O. Lüders, and R. John Leigh. Effects of eyelid closure, blinks, and eye movements on the electroencephalogram. *Clinical Neurophysiology*, 116(4):878–885, 2005.

[41] Sebastian Halder, Michael Bensch, Jürgen Mellinger, Martin Bogdan, Andrea Kübler, Niels Birbaumer, and Wolfgang Rosenstiel. Online artifact removal for brain-computer interfaces using support vector machines and blind source separation. *Computational intelligence and neuroscience*, 2007, 2007.

[42] Mohammed Abo-Zahhad, Sabah Ahmed, and Sherif Nagib Seha. A new eeg acquisition protocol for biometric identification using eye blinking signals. *International Journal of Intelligent Systems and Applications (IJISA)*, 07:48–54, 05 2015.

[43] Alon Keren, Shlomit Yuval-Greenberg, and Leon Deouell. Keren as, yuval-greenberg s, deouell ly. saccadic spike potentials in gamma-band eeg: characterization, detection and suppression. neuroimage 49: 2248-2263. *NeuroImage*, 49:2248–63, 10 2009.

[44] Sung-Phil Kim. Preprocessing of eeg. *Computational EEG Analysis: Methods and Applications*, pages 15–33, 2018.

[45] Tapio Saramäki, SK Mitra, and JF Kaiser. Finite impulse response filter design. *Handbook for digital signal processing*, 4:155–277, 1993.

[46] Edmund Lai. 8 - digital filter realizations. In Edmund Lai, editor, *Practical Digital Signal Processing*, pages 171–203. Newnes, Oxford, 2003.

[47] Charvi A Majmudar, Ruhi Mahajan, and Bashir I Morshed. Real-time hybrid ocular artifact detection and removal for single channel eeg. In *2015 IEEE International Conference on Electro/Information Technology (EIT)*, pages 330–334. IEEE, 2015.

[48] Amara Graps. An introduction to wavelets. *IEEE computational science and engineering*, 2(2):50–61, 1995.

[49] Luis Alfredo Moctezuma. *Towards Universal EEG systems with minimum channel count based on Machine Learning and Computational Intelligence.* Doctoral thesis, Norwegian University of Science and Technology, Trondheim, August 2021.

[50] CD Tesche, MA Uusitalo, RJ Ilmoniemi, M Huotilainen, M Kajola, and O Salonen. Signal-space projections of meg data characterize both distributed and well-localized neuronal sources. *Electroencephalography and clinical neurophysiology*, 95(3):189–200, 1995.

[51] Niels Trusbak Haumann, Lauri Parkkonen, Marina Kliuchko, Peter Vuust, and Elvira Brattico. Comparing the performance of popular meg/eeg artifact correction methods in an evoked-response study. *Computational Intelligence and Neuroscience*, 2016, 2016.

[52] MNE Developers. Signal-space projection (ssp), 2018.

[53] Ganesh R Naik and Dinesh K Kumar. An overview of independent component analysis and its applications. *Informatica*, 35(1), 2011.

[54] Pierre Comon. Independent component analysis, a new concept? *Signal processing*, 36(3):287–314, 1994.

[55] Ian Goodfellow, Yoshua Bengio, and Aaron Courville. *Deep Learning*. MIT Press, 2016. `http://www.deeplearningbook.org`.

[56] Ethem Alpaydin. *Machine learning: the new AI*. MIT press, 2016.

[57] K Palani Thanaraj, B Parvathavarthini, U John Tanik, V Rajinikanth, Seifedine Kadry, and Krishnamurthy Kamalanand. Implementation of deep neural networks to classify eeg signals using gramian angular summation field for epilepsy diagnosis. *arXiv preprint arXiv:2003.04534*, 2020.

[58] Barry J Wythoff. Backpropagation neural networks: a tutorial. *Chemometrics and Intelligent Laboratory Systems*, 18(2):115–155, 1993.

[59] Robert Hecht-Nielsen. Theory of the backpropagation neural network. In *Neural networks for perception*, pages 65–93. Elsevier, 1992.

[60] Judith E Dayhoff and James M DeLeo. Artificial neural networks: opening the black box. *Cancer: Interdisciplinary International Journal of the American Cancer Society*, 91(S8):1615–1635, 2001.

[61] Jonas Teuwen and Nikita Moriakov. Convolutional neural networks. In *Handbook of medical image computing and computer assisted intervention*, pages 481–501. Elsevier, 2020.

[62] Saad Albawi, Tareq Abed Mohammed, and Saad Al-Zawi. Understanding of a convolutional neural network. In *2017 international conference on engineering and technology (ICET)*, pages 1–6. Ieee, 2017.

[63] VERONICA JOHANSSON, SURJO R. SOEKADAR, and JENS CLAUSEN. Locked out: Ignorance and responsibility in brain–computer interface communication in locked-in syndrome. *Cambridge Quarterly of Healthcare Ethics*, 26(4):555–576, 2017.

[64] Zulay R. Lugo, Marie-Aurélie Bruno, Olivia Gosseries, Athena Demertzi, Lizette Heine, Marie Thonnard, Véronique Blandin, Frédéric Pellas, and Steven Laureys. Beyond the gaze: Communicating in chronic locked-in syndrome. *Brain Injury*, 29(9):1056–1061, 2015. PMID: 26182228.

[65] Mariana P Branco, Elmar GM Pels, Femke Nijboer, Nick F Ramsey, and Mariska J Vansteensel. Brain-computer interfaces for communication: preferences of individuals with locked-in syndrome, caregivers and researchers. *Disability and Rehabilitation: Assistive Technology*, pages 1–11, 2021.

[66] Mikhail A Lebedev and Miguel AL Nicolelis. Brain-machine interfaces: From basic science to neuroprostheses and neurorehabilitation. *Physiological reviews*, 97(2):767–837, 2017.

[67] Nataliya Kosmyna, Franck Tarpin-Bernard, Nicolas Bonnefond, and Bertrand Rivet. Feasibility of bci control in a realistic smart home environment. *Frontiers in Human Neuroscience*, 10, 2016.

[68] Ujwal Chaudhary, Ioannis Vlachos, Jonas B Zimmermann, Arnau Espinosa, Alessandro Tonin, Andres Jaramillo-Gonzalez, Majid Khalili-Ardali, Helge Topka, Jens Lehmberg, Gerhard M Friehs, et al. Spelling interface using intracortical signals in a completely locked-in patient enabled via auditory neurofeedback training. *Nature communications*, 13(1):1236, 2022.

[69] Tomislav Milekovic, Anish A Sarma, Daniel Bacher, John D Simeral, Jad Saab, Chethan Pandarinath, Brittany L Sorice, Christine Blabe, Erin M Oakley, Kathryn R Tringale, et al. Stable long-term bci-enabled communication in als and locked-in syndrome using lfp signals. *Journal of neurophysiology*, 120(7):343–360, 2018.

[70] Yoji Okahara, Kouji Takano, Masahiro Nagao, Kiyohiko Kondo, Yasuo Iwadate, Niels Birbaumer, and Kenji Kansaku. Long-term use of a neural prosthesis in progressive paralysis. *Scientific reports*, 8(1):16787, 2018.

[71] Hubert Cecotti. A self-paced and calibration-less ssvep-based brain–computer interface speller. *IEEE transactions on neural systems and rehabilitation engineering*, 18(2):127–133, 2010.

[72] Faraz Akram, Hee-Sok Han, and Tae-Seong Kim. A p300-based brain computer interface system for words typing. *Computers in biology and medicine*, 45:118–125, 2014.

[73] Xiaogang Chen, Yijun Wang, Masaki Nakanishi, Xiaorong Gao, Tzyy-Ping Jung, and Shangkai Gao. High-speed spelling with a noninvasive brain–computer interface. *Proceedings of the national academy of sciences*, 112(44):E6058–E6067, 2015.

[74] Rifai Chai, Sai Ho Ling, Gregory P Hunter, Yvonne Tran, and Hung T Nguyen. Brain–computer interface classifier for wheelchair commands using neural network with fuzzy particle swarm optimization. *IEEE journal of biomedical and health informatics*, 18(5):1614–1624, 2013.

[75] Daniel Ashley Craig and HT Nguyen. Adaptive eeg thought pattern classifier for advanced wheelchair control. In *2007 29th Annual International Conference of the IEEE Engineering in Medicine and Biology Society*, pages 2544–2547. IEEE, 2007.

[76] Jinyi Long, Yuanqing Li, Hongtao Wang, Tianyou Yu, Jiahui Pan, and Feng Li. A hybrid brain computer interface to control the direction and speed of a simulated or real wheelchair. *IEEE Transactions on Neural Systems and Rehabilitation Engineering*, 20(5):720–729, 2012.

[77] Bruce Denby, Tanja Schultz, Kiyoshi Honda, Thomas Hueber, Jim M Gilbert, and Jonathan S Brumberg. Silent speech interfaces. *Speech Communication*, 52(4):270–287, 2010.

[78] Frank H Guenther and Jonathan S Brumberg. Brain-machine interfaces for real-time speech synthesis. In *2011 Annual International Conference of the IEEE Engineering in Medicine and Biology Society*, pages 5360–5363. IEEE, 2011.

[79] Christian J Bell, Pradeep Shenoy, Rawichote Chalodhorn, and Rajesh PN Rao. Control of a humanoid robot by a noninvasive brain–computer interface in humans. *Journal of neural engineering*, 5(2):214, 2008.

[80] Yongwook Chae, Jaeseung Jeong, and Sungho Jo. Toward brain-actuated humanoid robots: asynchronous direct control using an eeg-based bci. *IEEE Transactions on Robotics*, 28(5):1131–1144, 2012.

[81] Pierre Gergondet, Sebastien Druon, Abderrahmane Kheddar, Christoph Hintermüller, Christoph Guger, and Mel Slater. Using brain-computer interface to steer a humanoid robot. In *2011 IEEE International Conference on Robotics and Biomimetics*, pages 192–197. IEEE, 2011.

[82] Mehrdad Fatourechi, Ali Bashashati, Rabab K Ward, and Gary E Birch. Emg and eog artifacts in brain computer interface systems: A survey. *Clinical neurophysiology*, 118(3):480–494, 2007.

[83] Shailaja Kotte and J R K Kumar Dabbakuti. Methods for removal of artifacts from eeg signal: A review. *Journal of Physics: Conference Series*, 1706(1):012093, dec 2020.

[84] Ahmad Mayeli, Vadim Zotev, Hazem Refai, and Jerzy Bodurka. Real-time eeg artifact correction during fmri using ica. *Journal of Neuroscience Methods*, 274:27–37, 2016.

[85] Saleha Khatun, Ruhi Mahajan, and Bashir I. Morshed. Comparative study of wavelet-based unsupervised ocular artifact removal techniques for single-channel eeg data. *IEEE Journal of Translational Engineering in Health and Medicine*, 4:1–8, 2016.

[86] Simen Fløtaker, Marta Molinas, and Andres Soler. Deep learning for classification of primary color responses in eeg signals using source reconstruction, 2022.

[87] Alexandre Gramfort, Martin Luessi, Eric Larson, Denis A. Engemann, Daniel Strohmeier, Christian Brodbeck, Roman Goj, Mainak Jas, Teon Brooks, Lauri Parkkonen, and Matti S. Hämäläinen. MEG and EEG data analysis with MNE-Python. *Frontiers in Neuroscience*, 7(267):1–13, 2013.

[88] Pauli Virtanen, Ralf Gommers, Travis E. Oliphant, Matt Haberland, Tyler Reddy, David Cournapeau, Evgeni Burovski, Pearu Peterson, Warren Weckesser, Jonathan Bright, Stéfan J. van der Walt, Matthew Brett, Joshua Wilson, K. Jarrod Millman, Nikolay Mayorov, Andrew R. J. Nelson, Eric Jones, Robert Kern, Eric Larson, C J Carey, İlhan Polat, Yu Feng, Eric W. Moore, Jake VanderPlas, Denis Laxalde, Josef Perktold, Robert Cimrman, Ian Henriksen, E. A. Quintero, Charles R. Harris, Anne M. Archibald, Antônio H. Ribeiro, Fabian Pedregosa, Paul van Mulbregt, and SciPy 1.0 Contributors. SciPy 1.0: Fundamental Algorithms for Scientific Computing in Python. *Nature Methods*, 17:261–272, 2020.

[89] Gregory Lee, Ralf Gommers, Filip Waselewski, Kai Wohlfahrt, and Aaron O'Leary. Pywavelets: A python package for wavelet analysis. *Journal of Open Source Software*, 4(36):1237, 2019.

[90] Charles R. Harris, K. Jarrod Millman, Stéfan J. van der Walt, Ralf Gommers, Pauli Virtanen, David Cournapeau, Eric Wieser, Julian Taylor, Sebastian Berg, Nathaniel J. Smith, Robert Kern, Matti Picus, Stephan Hoyer, Marten H. van Kerkwijk, Matthew Brett, Allan Haldane, Jaime Fernández del Río, Mark Wiebe, Pearu Peterson, Pierre Gérard-Marchant, Kevin Sheppard, Tyler Reddy, Warren Weckesser, Hameer Abbasi, Christoph Gohlke, and Travis E. Oliphant. Array programming with NumPy. *Nature*, 585(7825):357–362, September 2020.

[91] Vlawhern. This is the army research laboratory (arl) eegmodels project: A collection of convolutional neural network (cnn) models for eeg signal classification, using keras and tensorflow. `https://github.com/vlawhern/arl-eegmodels`, Year.

[92] P Senthil Kumar, R Arumuganathan, K Sivakumar, and C Vimal. Removal of ocular artifacts in the eeg through wavelet transform without using an eog reference channel. *Int. J. Open Problems Compt. Math*, 1(3):188–200, 2008.

[93] Alejandro Antonio Torres-García and Marta Molinas. Analyzing the recognition of color exposure and imagined color from eeg signals. In *2019 IEEE 19th International Conference on Bioinformatics and Bioengineering (BIBE)*, pages 386–391. IEEE, 2019.

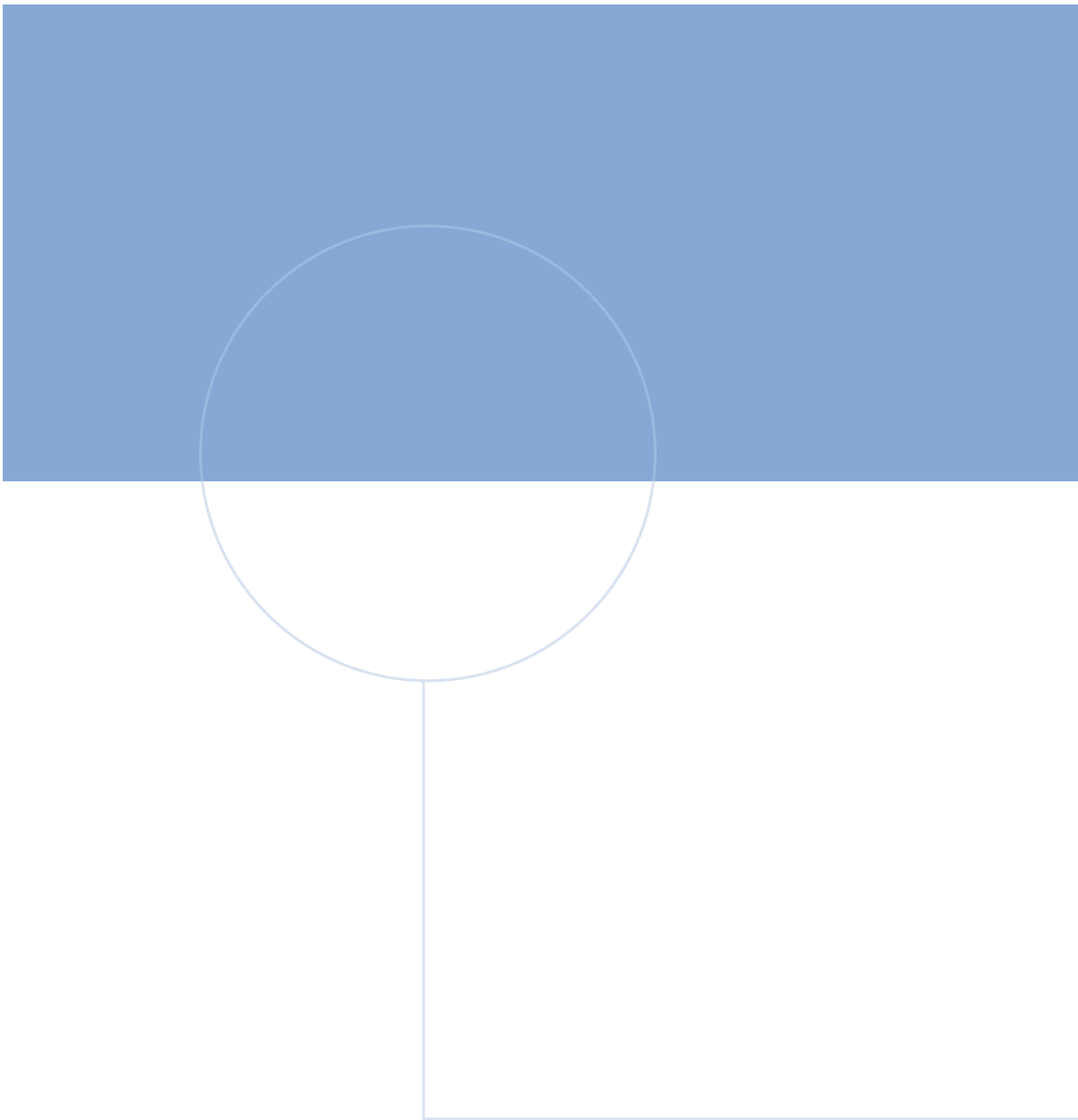

NTNU

Norwegian University of
Science and Technology